1.0

2.8 2.5

3.2 2.2

2.0

1.1

1.8

1.25 1.4 1.6

MICROCOPY RESOLUTION TEST CHART

LEVEL

DNA 5578F

SGEMP ANALYSIS USING THE PROGRAMMABLE CALCULATOR

A. J. Woods

R. E. Leadon

B. Nichols

K. Brannon

E. P. Wenaas

JAYCOR

P. O. Box 85154

San Diego, California 92138

DTIC
ELECTE
JAN 1 8 1982
B

30 August 1980

Final Report for Period 1 March 1979—1 June 1980

CONTRACT No. DNA 001-79-C-0209

APPROVED FOR PUBLIC RELEASE;
DISTRIBUTION UNLIMITED.

Prepared for

Director

DEFENSE NUCLEAR AGENCY

Washington, D. C. 20305

REPORT DOCUMENTATION PAGE		READ INSTRUCTIONS BEFORE COMPLETING FORM
1. REPORT NUMBER DNA 5578F	2. GOVT ACCESSION NO. AD-A109 680	3. RECIPIENT'S CATALOG NUMBER
4. TITLE (and Subtitle) SGEMP ANALYSIS USING THE PROGRAMMABLE CALCULATOR		5. TYPE OF REPORT & PERIOD COVERED Final Report for Period 1 Mar 79—1 Jun 80
		6. PERFORMING ORG. REPORT NUMBER 200-80-238-2150
7. AUTHOR(s) A. J. Woods K. Brannon R. E. Leadon E. P. Wenaas B. Nichols		8. CONTRACT OR GRANT NUMBER(s) DNA 001-79-C-0209
9. PERFORMING ORGANIZATION NAME AND ADDRESS JAYCOR P. O. Box 85154 San Diego, California 92138		10. PROGRAM ELEMENT PROJECT TASK AREA & WORK UNIT NUMBERS Subtask R99QAXEE502-25
11. CONTROLLING OFFICE NAME AND ADDRESS Director Defense Nuclear Agency Washington, D. C. 20305		12. REPORT DATE 30 August 1980
		13. NUMBER OF PAGES 92
14. MONITORING AGENCY NAME & ADDRESS(if different from Controlling Office)		15. SECURITY CLASS. (of this report) UNCLASSIFIED
		15a. DECLASSIFICATION DOWNGRADING SCHEDULE N/A

16. DISTRIBUTION STATEMENT (of this Report)

Approved for public release; distribution unlimited.

17. DISTRIBUTION STATEMENT (of the abstract entered in Block 20, if different from Report)

18. SUPPLEMENTARY NOTES

This work sponsored by the Defense Nuclear Agency under
RDT&E RMSS Code B323079464 R99QAXEE50225 H2590D.

19. KEY WORDS (Continue on reverse side if necessary and identify by block number)

SGEMP	Electron Emission
TI-59	Electromagnetic Fields
Programmable Calculator Codes	Cable Response
X-ray Attenuation	Satellite Response

20. ABSTRACT (Continue on reverse side if necessary and identify by block number)

An analysis package developed for the quantification of SGEMP effects on the Texas Instruments TI-59 programmable calculator is described. The code system is designed for use on a standard calculator using magnetic card inputs, and enables the analyst to attenuate x-ray spectra to a continuum of satellite locations, generate photoemission excitation parameters, and evaluate electromagnetic fields and cable current drivers. Calculations can be made on both the exterior and interior of the vehicle for a variety of electron emission

20. ABSTRACT (Continued)

materials and x-ray environments producing both linear and space-charge-limited responses. Accuracy of the results is within a factor of 5 or better compared to complex computer calculations over ranges of x-ray environments of interest for satellite SGEMP. Example SGEMP analyses performed with the calculator and complete user's instructions are described.

TABLE OF CONTENTS

1

LIST OF ILLUSTRATIONS

1. INTRODUCTION

System-generated electromagnetic pulse (SGEMP) effects on space vehicles have been addressed with extensive analytical and experimental efforts. Complex analytical models have been developed and tested against experimental results, and key SGEMP parameters and hardening methods have been identified. Considerable additional effort is still needed in applying the science to military systems, however, and a means of efficiently identifying system weaknesses to SGEMP effects would be valuable. Present analyses of systems are generally conducted by a team of specialists employing analytical and computer-aided methods in conjunction with experimental efforts. However, extensive training in the field is required to perform an analysis, and in fact, military systems may evolve faster than the present methods would permit estimations of hardness to SGEMP.

This report presents an SGEMP analysis system designed to aid in rapidly scoping SGEMP effects. A set of analytical models is solved on a programmable calculator, giving numerical evaluations of important parameters that characterize SGEMP response. The user must be familiar only with parameters describing the x-ray environment and system geometry. Details of SGEMP modeling are handled by the calculator codes. Output parameters such as electromagnetic fields and cable current driver values permit the analyst to determine magnitudes of effects and their sensitivity to various parameters. The calculator codes are useful to the experienced SGEMP specialist, and also enable the novice to identify potential areas of SGEMP vulnerability for a particular system and x-ray environment.

The degree of accuracy which may be achieved on the calculator is best illustrated by comparing results with more complex calculations. Figure 1 shows peak external replacement current magnitudes on a cylinder subjected to a variety of x-ray spectra and fluence levels. The curves were obtained at considerable expense (~10 hours of CDC CYBER-176 computer time using 300,000 60-bit words of memory), using the 2-1/2-dimensional ABORC computer code, and at considerably less expense (~20 minutes of execution time using 120 words of memory) with the Texas Instruments TI-59 calculator. The agreement between the two methods is a factor of 2 over problem conditions ranging from non-space-charge-limited to highly space-charge-limited. This quality of results can

3
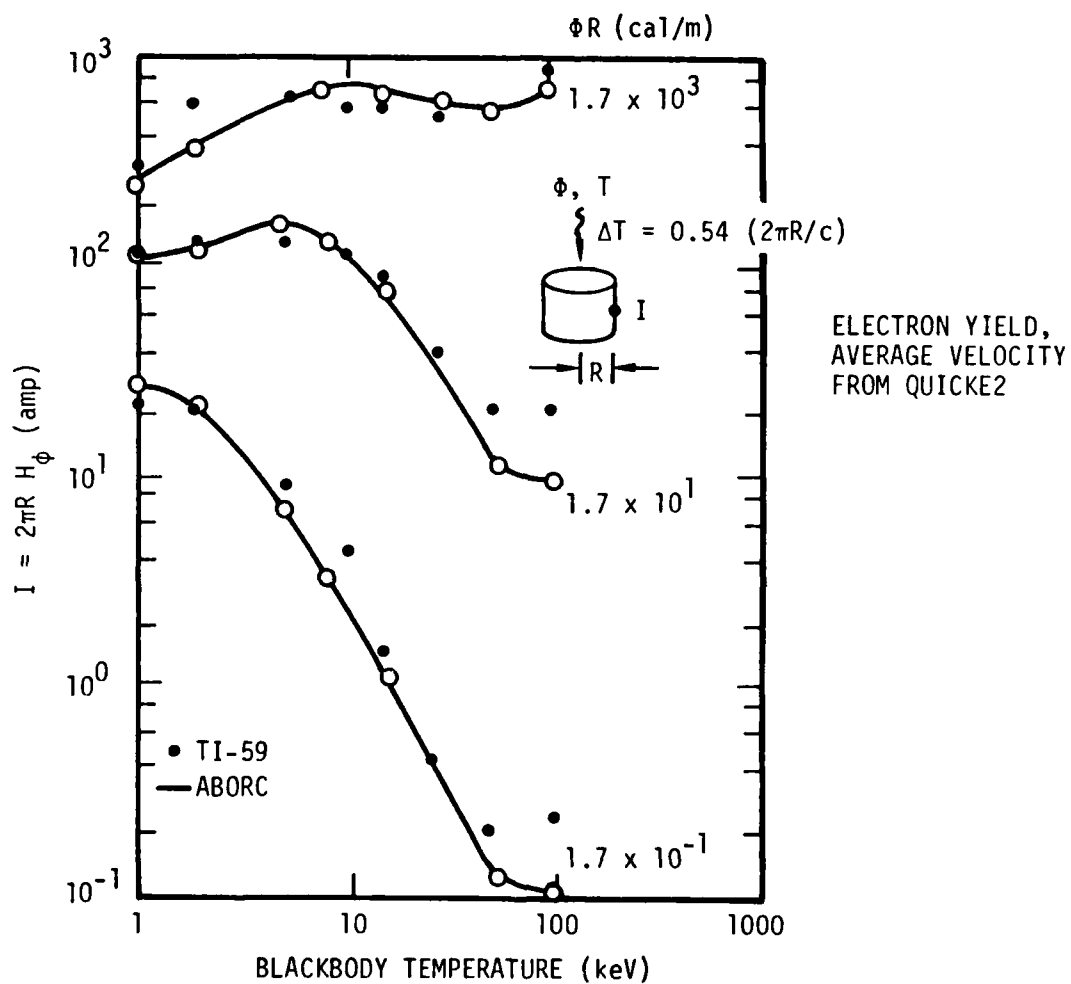
Figure 1. Peak surface currents versus spectrum temperature for
different fluence products in cal/m. Solutions apply for
a pulse time Δt = 0.54(2πR/c), where c is the speed of light.
The x-ray pulse rise time was ≈ 0.6 x Δt.

RE-03192

4

probably be achieved in most SGEMP areas discussed here, although certain calculational areas require some additional development to achieve the quality shown in Figure 1. Additional comparisons of the external response of the cylinder with ABORC results are found in Section 5, along with an explanation of the scaled format in which the results are presented.

The analysis tools presented here form a unified package which allows SGEMP assessment beginning with the x-ray environment and ending with cable current drivers. The package is complete in that each major SGEMP area can be scoped with the codes. The required analysis leading to estimates for fields and cable currents is summarized as follows. First, the x-ray spectrum is attenuated to the satellite location of interest. Data bases are used to calculate values for electron photoemission yield, average velocity, and the dipole moment in dielectrics. These results are then employed in equations for the peak time rates of change of the electric field and the space-charge dipole moment near an emitting surface. Finally, simplified expressions are evaluated for the cable current driver terms.

Emphasis in the present program has been on providing an analytical tool based on the development of the field of SGEMP analysis to date. The analytical models discussed in this report allow estimates to be made for electromagnetic fields in the non-linear fluence regimes -- for example, where the physics is understood but the formulas are usually too complex to be solved by hand in a practical manner. Calculator results can be obtained within a matter of minutes, with only modest effort required of the analyst. Quick-response SGEMP assessments with nontrivial input parameters can be performed with the system. Potential applications include evaluation of candidate x-ray simulator spectra for SGEMP effects and the determination of principal cable current driver mechanisms for a given threat environment and satellite orientation.

The calculator codes here are a generalized extension of work reported earlier (Ref. 1). The analysis system described in Reference 1 was limited to preselected satellite positions and emission materials, and stopped short of the electromagnetic field and cable coupling capablities available with the present system.

Model development to date has been for solution of satellite materials, environments, and x-ray threat parameters. The particular codes discussed here were thus designed for the parameter ranges and physics of the satellite problem. They can be applied to other problems as well, such as missile and ground systems. However, some

important physical effects will not be calculated in those cases. For example, air chemistry effects important at lower altitudes are not included in the models, and x-ray energies are limited to 1 MeV in the data base (which is slightly lower than the range of interest for ground systems).

The remainder of this report is organized as follows. Section 2 provides a review of SGEMP phenomenology and satellite system analysis methods. Section 3 discusses the approach to simplification of SGEMP for the calculator for each analysis step and also notes the related phenomena not covered by the programs. Section 4 then gives an overview of the modeling approach for each category of SGEMP analysis. In Section 5, capabilities of the resultant calculator system are demonstrated through comparisons with more complex calculations. A summary of capabilities is given in Section 6, which includes quantitative accuracy estimates and a list of modeling limitations.

Details of the modeling of effects are found in Appendix A. Complete user instructions for the codes are given in Appendix B, along with a detailed example problem. Graphs of the photoemission excitation parameter data base are provided in Appendix C.

2. REVIEW OF SGEMP PHENOMENOLOGY AND SYSTEM ANALYSIS METHODS

The SGEMP problem is illustrated in Figure 2. An x-ray environment specified by a time-dependent energy spectrum and flux is incident on a satellite system. Photoemission due to the x rays occurs on and throughout the structure, inducing currents in the electronics. Satellite locations representative of important sources of cable currents in the system are identified in the figure.

Lack of attenuation on the outside of the vehicle can cause very large currents, which must be prevented from coupling to the inside. Moderate attenuation into large cavities can cause substantial fields inside the vehicle which may drive currents on cable shields. Highly attenuated x rays can cause response in sensitive locations such as an electronic equipment box. Also, x rays drive currents directly in the cables through photoemission from shield materials, penetrating dielectrics, or gaps within the shield. Thus, both high and low x-ray fluence locations can be significant in causing currents in the sensitive electronics.

Coupling of currents into cables occurs by processes of knock-on current, $\dot{B}A$ voltage, $C\dot{V}$ current, and photon-driven current. In this discussion, the word "cable" can mean the conductor of an unshielded cable, the conducting sheath of a shielded cable, or the outer conducting shield around a cable bundle. "Direct drve" is also used to describe the photon-driven current.

The knock-on current is the net flux of photoelectrons captured or emitted by the cable sheath. The $\dot{B}A$ voltage source is due to a time-rate-of-change of magnetic flux enclosed by a cable loop. The $C\dot{V}$ current source results from the time-rate-of-change of the voltage between a cable and another conductor, where C is the mutual capacitance. Finally, the photon-driven current is the result of the displacement of charge emitted from cable conductors and lodging in dielectric insulators (usually identified with the inside of a shielded cable).

Other sources of currents caused by the weapon include dielectric charging and penetration of charge due to the enhanced electron environment.

The contributions of the different phenomenology processes to the total system response are illustrated in Figure 3. The boxes represent calculation steps which must be performed in analyzing a system. X-ray transport and photoelectron emission are fundamental to each cable driver process shown in the second layer of boxes. Resultant
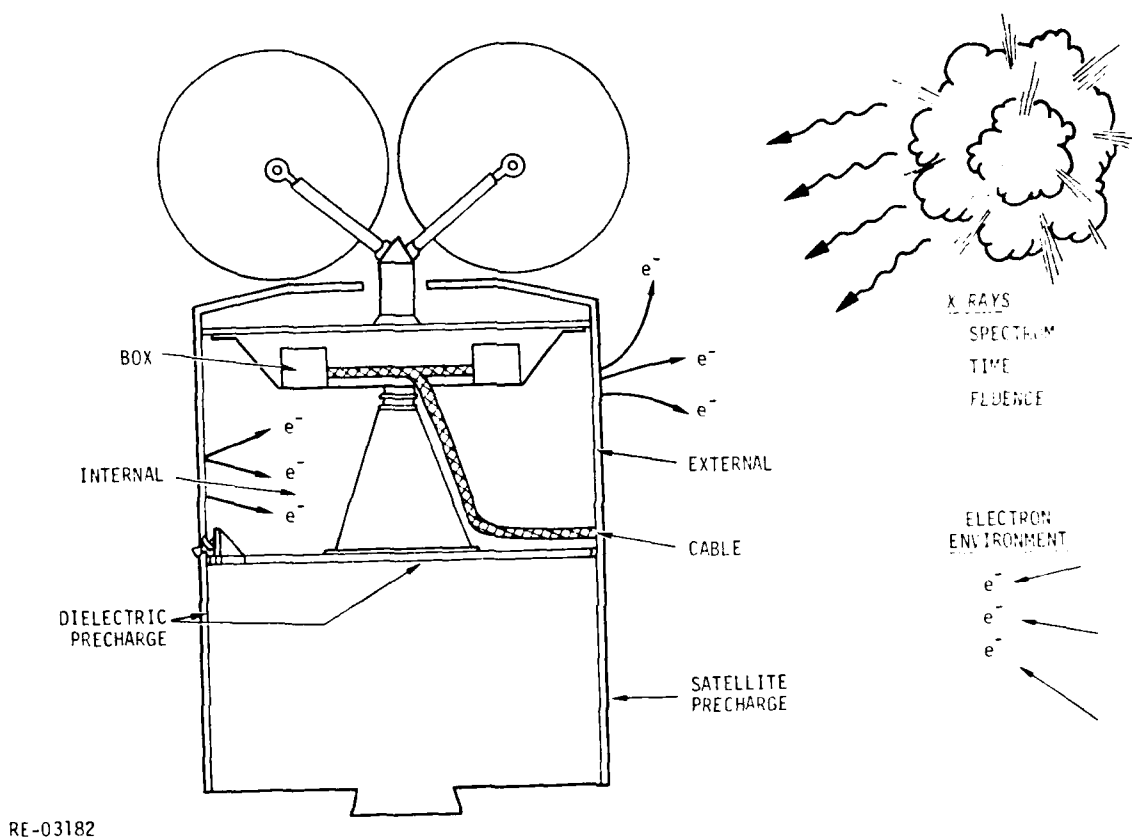
Figure 2. SGEMP response phenomenology
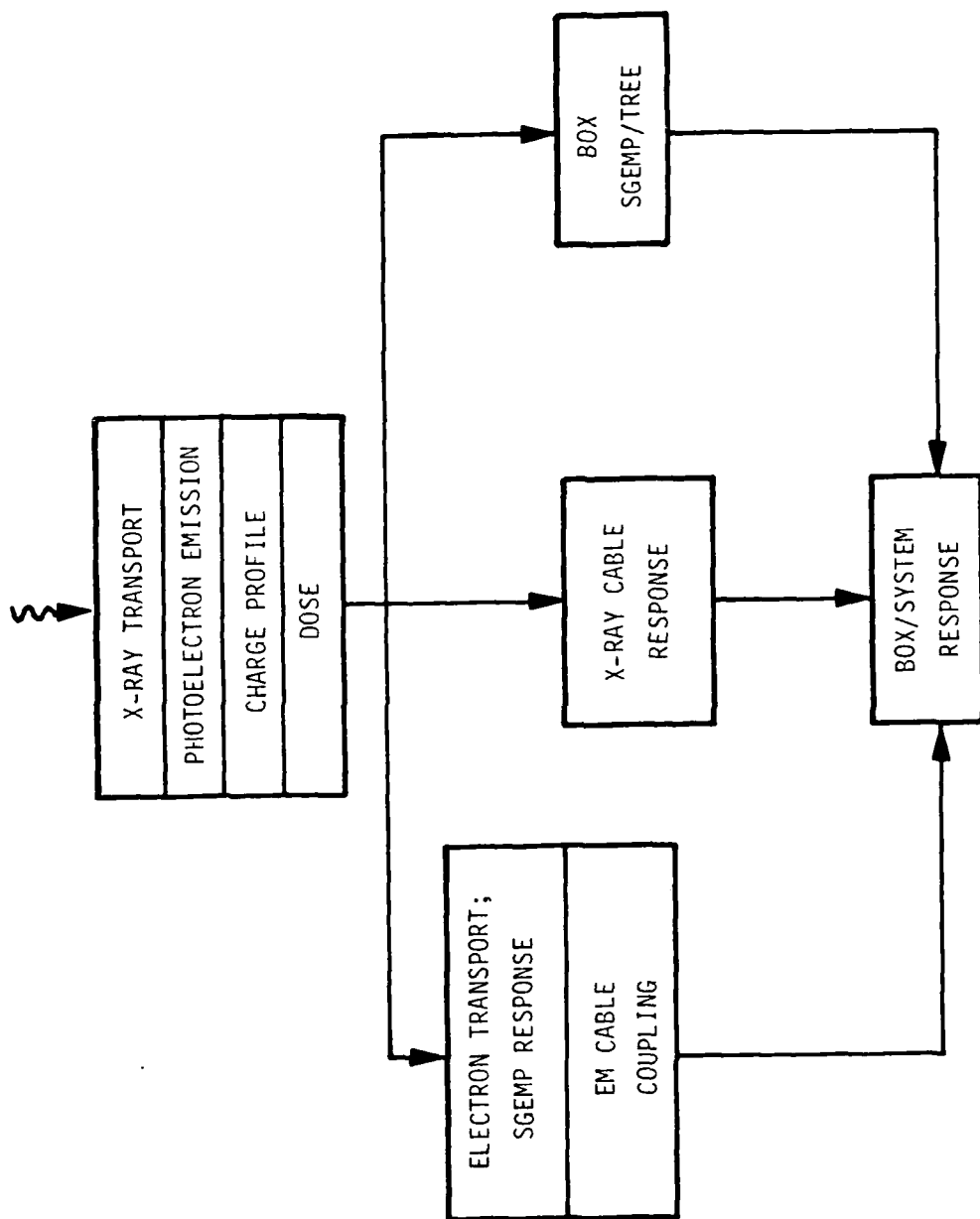
RE-03182

Figure 3. Phenomenology processes contributing to system response

RE-03183

9

energetic electrons couple into cables and electronics by means of electromagnetic fields, direct x-ray effects inside cable shields, and effects inside equipment boxes themselves. The total system response is obtained by simultaneously combining each of the effects into an electrical model of the whole.

3. SIMPLIFICATION OF SGEMP FOR THE CALCULATOR

The approach taken in model development for the calculator is typical of that followed when a full-scale computer is being used. The problem complexity or detail of solution is adjusted to available resources, of which memory size and execution time are usually the most critical. Data bases are often employed to describe essential inputs which are not the object of the investigation, and detailed solutions of models containing the parameters under investigation are solved using a combination of analytical and numerical techniques.

The calculator has many of the attributes of a large computer, the principal differences being memory size and execution speed. In general, greater reliance is placed on analytical assumptions and interpolations than would be necessary on a large computer, but the models can achieve considerable complexity and still be solvable within a minute or so of execution time. The models described here were developed employing key SGEMP parameters for simplified configurations, with reliance on curve-fitting to precomputed results limited to the photoelectron excitation parameters.

X-ray transport is computed for incident spectra using exponential attenuation, with a simplified expression for the mass absorption coefficients for all materials. Photoelectron parameters are obtained from convolution of attenuated spectra with a precomputed data base. Electromagnetic response parameters obtained from simplifying assumptions for plane geometry are then applied to finite objects. Cable coupling terms are treated separately for each effect, ignoring synergistic possibilities. Knock-on current is computed disregarding the the cable's effect on space charge, for example. $\dot{C}V$ and $\dot{B}A$ coupling models employ a rod-over-ground plane ideal geometry, and the direct-drive model assumes a coaxial geometry.

Effects of spacecraft charging due to the enhanced nuclear electron environment are not modeled for the calculator at present, nor are discharges.

The present codes enable the user to compute individual cable current drivers as the highest level of SGEMP analysis. The models stop short of combining the drivers into an electrical model of the entire system, as illustrated by the lowest box in Figure 3. Such a model would suffer greatly from oversimplification with the present calculator resources due to the degree of coupling between spacecraft components. The cable current drivers are considered to be sufficient here for analyzing SGEMP effects with the present limitations of calculator resources.

11

4. OVERVIEW OF SGEMP MODELING FOR THE PROGRAMMABLE CALCULATOR

This section provides an overview of the modeling of the different SGEMP analysis steps for the calculator. A brief description of calculator capabilities is given to acquaint the reader with the size of the programs used to solve the models. The idealized analysis configuration is described, and the modeling approach for each division of SGEMP effects is highlighted. Various comments on the relevance of the analysis configurations and model completeness and accuracy are also made. Details of the modeling are discussed in Appendix A.

4.1 ALLOWABLE COMPLEXITY PERMITTED BY CALCULATOR MEMORY

The approach to the modeling has been to restrict allowable complexity so that all programs fit within the TI-59 calculator in the standard off-the-shelf configuration. Additional memory obtainable through use of a "chip" is not required, for example, and neither is a printer. Extension of the programs could be accomplished with more memory, of course, and increased accuracy and user convenience would be realized. At present, however, the available memory is assumed to be limited to the standard 960 program steps. (A program step represents a single key stroke on the calculator such as a multiply or storage operation.)

Calculator memory can be partitioned variably between storage of data or program steps, with a single data number occupying the space of eight program steps. Divisions of memory have been varied for different aspects of the SGEMP problem in the programs reported here. For example, photon attenuation and excitation parameter calculations require manipulation of a photon spectrum, and the calculator stores considerable data but employs relatively simple programs. The memory division is 240 program steps and 90 data locations in those cases. Electromagnetic response parameters require relatively few data inputs, but more complex programs. In that case, the calculator memory is divided into 560 program steps and 50 data locations.

In all cases, storage is severely limited when 50 to 90 data locations are compared against the currently available 420,000 60-bit words on the DNA CYBER-176 computer, where most of the world's SGEMP calculations have been conducted to date.

Considering the limitations of calculator memory, the SGEMP problem has been broken into four divisions which are treated by separate programs. The divisions are:

photon attenuation, photoelectric excitation, electromagnetic response, and cable coupling. The programs are executed sequentially by reading in a different card(s) between divisions. This procedure is a tradeoff between problem resolution and operational convenience. Additionally, a user will, in many cases, be concerned with certain of the problem divisions more than others in an analysis. He may attenuate his spectrum through a thermal blanket only once, for example, and then evaluate the impact of changing the emission material or the incident fluence on fields in a cavity by using the attenuated spectrum repeatedly.

4.2   ANALYSIS CONFIGURATION

The idealized analysis configuration is illustrated in Figures 4 and 5. The first figure shows the parameters required to define the system for SGEMP effects. They describe the x-ray environment and the system geometry and material composition. The second figure gives the desired outputs from the models by which SGEMP effects are measured. The four cable current drivers are identified in Figure 5, along with other calculator outputs considered significant for determination of SGEMP effects. Notice that outputs are available both exterior and interior to the satellite model.

The cylindrical geometry shown in Figures 4 and 5 is employed to illustrate the relevant parameters for SGEMP effects. The calculator codes are not designed to solve the cylinder _per se_, but the results can, in general, be applied with reasonable accuracy to that geometry. It is convenient that major SGEMP drivers are not strongly dependent on object or cavity shapes for relatively simple geometries (Ref. 2). One-dimensional, planar geometry results often can be modified slightly and applied to much more complex shapes, especialy near photoemitting surfaces.

4.3   SUMMARIES OF MODELS FOR INDIVIDUAL ANALYSIS STEPS

4.3.1   X-Ray Attenuation

X-ray attenuation is treated the same as in most other SGEMP codes, except that it is scaled to the calculator memory size. A universal expression for the absorption coefficient is evaluated at each photon energy in the incident spectrum. The coefficients of the expression can be varied for accurately fitting data for a given material. Values employed here were based on the data of Biggs and Lighthill (Ref. 3). Accuracy is, in general, within a factor of 2 of more detailed calculations for typical satellite materials and
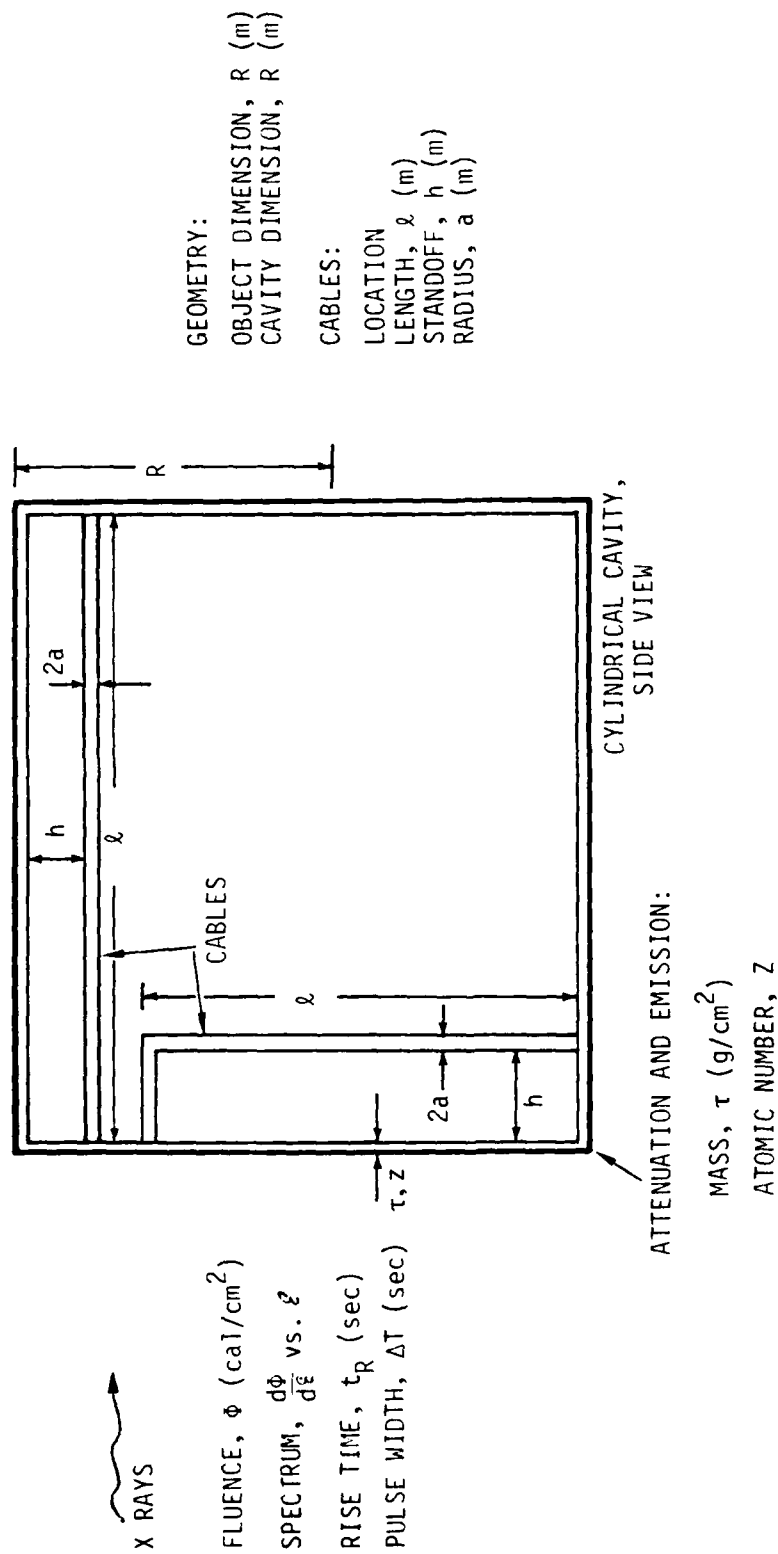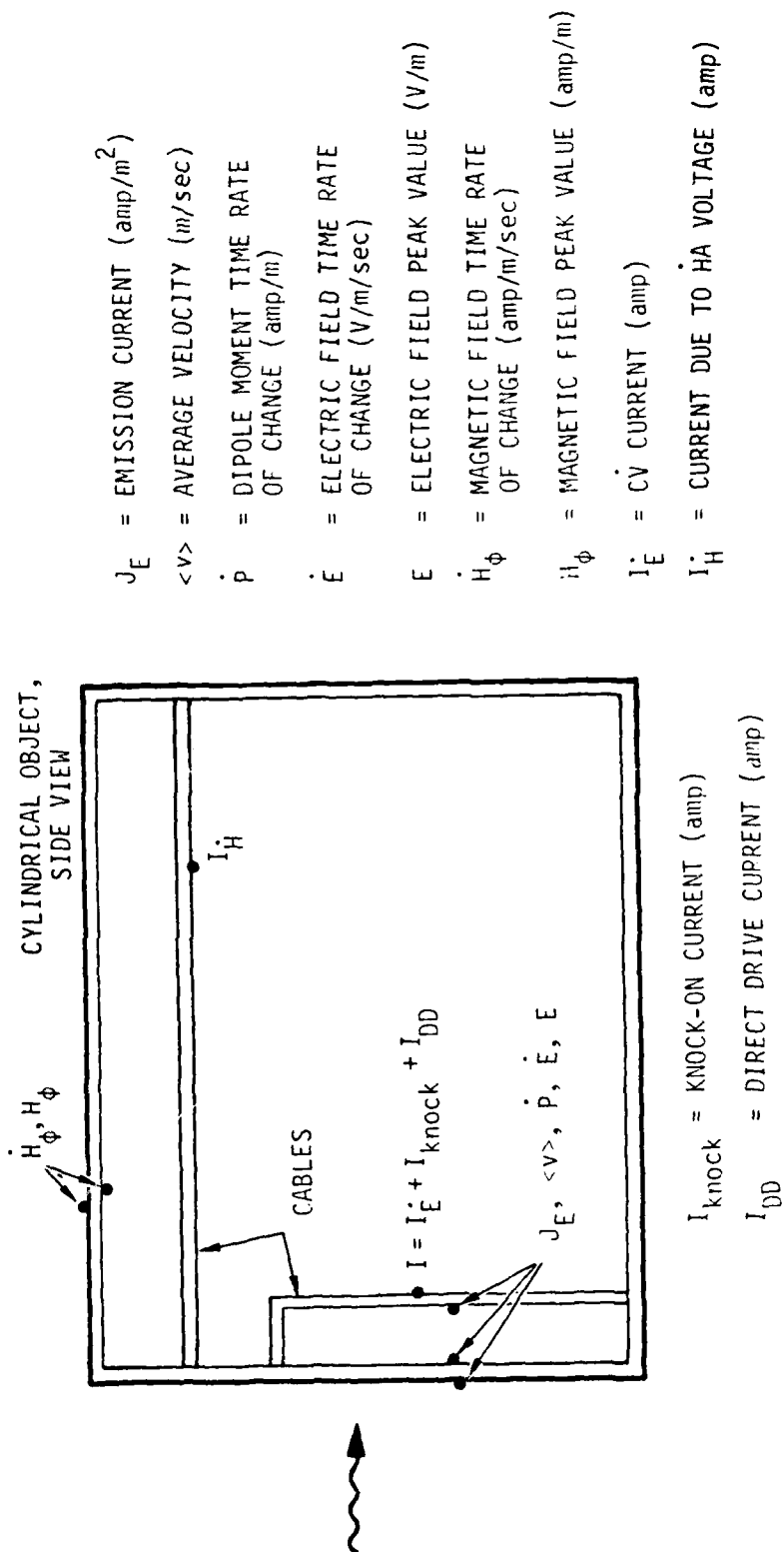
13

X RAYS

FLUENCE, Φ (cal/cm^2)

SPECTRUM, $\frac{d\Phi}{d\varepsilon}$ vs. ε

RISE TIME, t_R (sec)

PULSE WIDTH, ΔT (sec)

ATTENUATION AND EMISSION:

MASS, τ (g/cm^2)

ATOMIC NUMBER, Z

GEOMETRY:

OBJECT DIMENSION, R (m)
CAVITY DIMENSION, R (m)

CABLES:

LOCATION
LENGTH, ℓ (m)
STANDOFF, h (m)
RADIUS, a (m)

R

2a

h

ℓ

CABLES

ℓ

2a

h

τ, z

CYLINDRICAL CAVITY,
SIDE VIEW

Figure 4. Input parameters at the user's disposal for analyzing SGEMP response
in and around an idealized satellite model with calculator programs

RE-03091

14

CYLINDRICAL OBJECT, SIDE VIEW

$\dot{H}_\phi, H_\phi$

I_H

CABLES

$I = I_{\dot{E}} + I_{knock} + I_{DD}$

$J_E, <v>, \dot{P}, \dot{E}, E$

J_E = EMISSION CURRENT (amp/m^2)

$<v>$ = AVERAGE VELOCITY (m/sec)

$\dot{P}$ = DIPOLE MOMENT TIME RATE OF CHANGE (amp/m)

$\dot{E}$ = ELECTRIC FIELD TIME RATE OF CHANGE $(V/m/sec)$

E = ELECTRIC FIELD PEAK VALUE (V/m)

$\dot{H}_\phi$ = MAGNETIC FIELD TIME RATE OF CHANGE $(amp/m/sec)$

H_ϕ = MAGNETIC FIELD PEAK VALUE (amp/m)

$I_{\dot{E}}$ = $\dot{CV}$ CURRENT (amp)

$I_{\dot{H}}$ = CURRENT DUE TO $\dot{H}A$ VOLTAGE (amp)

I_{knock} = KNOCK-ON CURRENT (amp)

I_{DD} = DIRECT DRIVE CURRENT (amp)

RE-03092

Figure 5. SGEMP response characterization parameters from calculator programs

15

x-ray spectra (see Section 5). Exponential attenuation through parallel plates is performed based on the thickness and density of the material.

4.3.2   Photoemission Excitation

Photoemission excitation parameters (yield, average velocity, and dipole moment in dielectrics) are obtained by convolving the attenuated photon spectrum with energy-dependent data for monoenergetic photons obtained from the QUICKE2 photoemission code (Ref. 4). Data for a given parameter for a material resides on one side of a magnetic card and occupies one-fourth the calculator memory when it is read in. The convolution program performs power-law fits to the data base, giving excellent accuracy over the entire range of 1 to 1000 keV. Data are provided for representatives of the full range of satellite materials (listed in Appendix C).

4.3.3   Electromagnetic Response

Electromagnetic response parameters are obtained for a trapezoidal pulse of emission current from a single, isolated, conducting, floating, infinite plate. Simplifying assumptions of monoenergetic electrons emitted with a cosine angular distribution which are not allowed to mix spatially above the plate permit expressions for maximum values of the time-rates-of-change of the electric field and space-charge dipole moment ($\dot{E}$ and $\dot{P}$) to be solved analytically. (The approach is similar to those discussed in Refs. 5 and 6.) Identification of $\dot{P}$ as the principal driver of replacement currents on an idealized spherical geometry leads to an expression for the magnetic field, H. A quasi-static assumption leads to a peak value estimate of the electric field. The resultant expressions are too complex to permit practical evaluation by humans, but are well within the calculator's capability to solve rapidly. Comparison of results for planar geometry with a more exact particle-following computer code using actual electron spectra showed excellent agreement.

4.3.4   Cable Coupling

Cable coupling terms are provided for knock-on, $\dot{B}A$, $C\dot{V}$, and direct-drive effects. Knock-on current is taken to be simply the emitted current striking a cable shield from a nearby wall minus the current emitted from the shield. It is simplified by ignoring the effect of the cable on electron trajectories, so the results are most accurate at low fluence levels. $\dot{B}A$ drivers determine the current through a low-impedance loop using $\dot{B}$ obtained from $\ddot{P}$, the second time derivative of the space-charge dipole moment, and the

inductance of a cable above a ground plane. $C\dot{V}$ coupling employs the electromagnetic $\dot{E}$ term combined with the cable capacitance above a ground plane. The direct-drive term provides charge flow based on the dipole moment of electrons emitted from the outer shield into the dielectric insulator of a coaxial cable. Accuracy of the knock-on and direct-drive currents is most suspect, but all the terms give reasonable estimates of effects. The electromagnetic coupling terms are essentially the same as those commonly employed in more detailed analyses.

4.3.5   Summary of Modeling

Table 1 summarizes the conditions for which the various SGEMP models were developed. Table 2 summarizes characteristics of individual output parameters. Conditions and limiting assumptions are listed for each term, including the assumed geometry of the analytical model and the availability of a nonlinear (space-charge-limited) solution. Whereas the system covers many effects and conditions of interest, it must be exercized with some care as to interpretation of results for a given geometry and exposure environment. An overview of the expected accuracy of the system is presented in Section 6.

Table 1. Conditions for Which SGEMP Parameter Evaluation Models Were Developed

Calculation	Conditions
Photon attenuation	Photoelectric approximation
	All elements and combinations
	All satellite thicknesses
	All spectra from 1 to 1000 keV
Electron emission	Equivalent to QUICKE2 within accuracy of power-law fits
Yield	
Average velocity	
Dipole moment	

SGEMP fields

$\dot{E}$	Above single, floating, infinite ground plane
$\dot{P}$	Linear and nonlinear fluence regions
E	Trapezoidal pulse
H	Average normal electron velocity input
$\dot{H}$	Quasi-static

Cable current drivers

Knock-on	Unshielded cable above ground plane, coaxial cable for direct drive
$\dot{B}$	Cable does not perturb electron motion or fields
$\dot{CV}$	Linear and nonlinear fluence regimes
Direct drive	Short cables
	Low-impedance termination

18

Table 2. Output Parameter Characteristics Summary

Parameter	Exterior Solution?	Interior Solution?	Nonlinear Solution?	Geometry
Emission current, J_E	Yes	Yes	N/A	Plate
Average velocity, $\langle v \rangle$	Yes	Yes	N/A	Plate
Dipole moment rate, $\dot{P}$	Yes	Yes	Yes	Floating plate
Electric field rate, $\dot{E}$	Yes	Large cavity	Yes	Floating plate
Electric field, E	Yes	Large cavity	Yes	Floating plate
Magnetic field rate, $\dot{H}_\phi$	Yes	Pillbox	Exterior only	Sphere exterior, cylinder interior
Magnetic field, H_ϕ	Yes	Pillbox	Exterior only	Sphere exterior, cylinder interior
Knock-on current, I_{knock}	Yes	Yes	No	Cable over ground plane
$\dot{CV}$ current, $I_{\dot{E}}$	Yes	Yes	Exterior only	Cable over ground plane
Current from $\dot{H}A$ voltage, $I_{\dot{H}}$	Yes	Yes	Exterior only	Cable over ground plane
Direct-drive current, I_{DD}	Yes	Yes	N/A	Coaxial cable

5. SAMPLE SGEMP ANALYSES: COMPARISON OF CALCULATOR AND MULTIDIMENSIONAL COMPUTER CODE RESULTS

Example SGEMP analysis steps performed with the calculator codes are described in this section, and several comparisons are made with more detailed calculations. Accuracy of x-ray attenuation through representative satellite materials is compared with results from QUICKE2. Exterior response is calculated for a cylinder over wide ranges of x-ray parameters, and results are compared with the two-dimensional ABORC code (Ref. 7). A 1-m length=diameter inner cavity is analyzed and compared with ABORC, also. Finally, an electronics equipment box configuration is analyzed on the calculator, giving relative cable pickup magnitudes for a typical x-ray environment. The results serve both as illustrations of capabilities and as sample problems which aspiring analysts can use in practicing the routine.

5.1 BLACKBODY ATTENUATION BY SATELLITE MATERIALS

Calculations of blackbody spectra attenuated through representative satellite materials are compared with QUICKE2 code results in Figure 6. Agreement between the methods is within a factor of 2, even for the most difficult case of large attenuation through high-Z materials (shielded box). The calculator spectra were defined with 14 energy bins, and the QUICKE2 spectra had 50. The bin selection is much more critical for the highly attenuated cases than for the moderately attenuated cases. Notice that a multiple-plate case was performed on the calculator, also.

5.2 EXTERIOR RESPONSE OF A CYLINDER

The exterior response of a cylindrical object has been calculated with the TI-59 codes for a wide variety of incident x-ray environments. The results have been compared with published solutions from the ABORC code over ranges of x-ray fluence, time history, and energy spectrum (Ref. 8). The calculator codes employ specific geometry assumptions involving planar and spherical surfaces, whereas the ABORC results are for a cylinder. Previous analytical studies showed only moderate geometry sensitivity of SGEMP effects for relatively simple geometries (Ref. 2). Comparison between the calculator 'pseudo-sphere' and the ABORC cylinder should not be affected strongly by geometry differences.
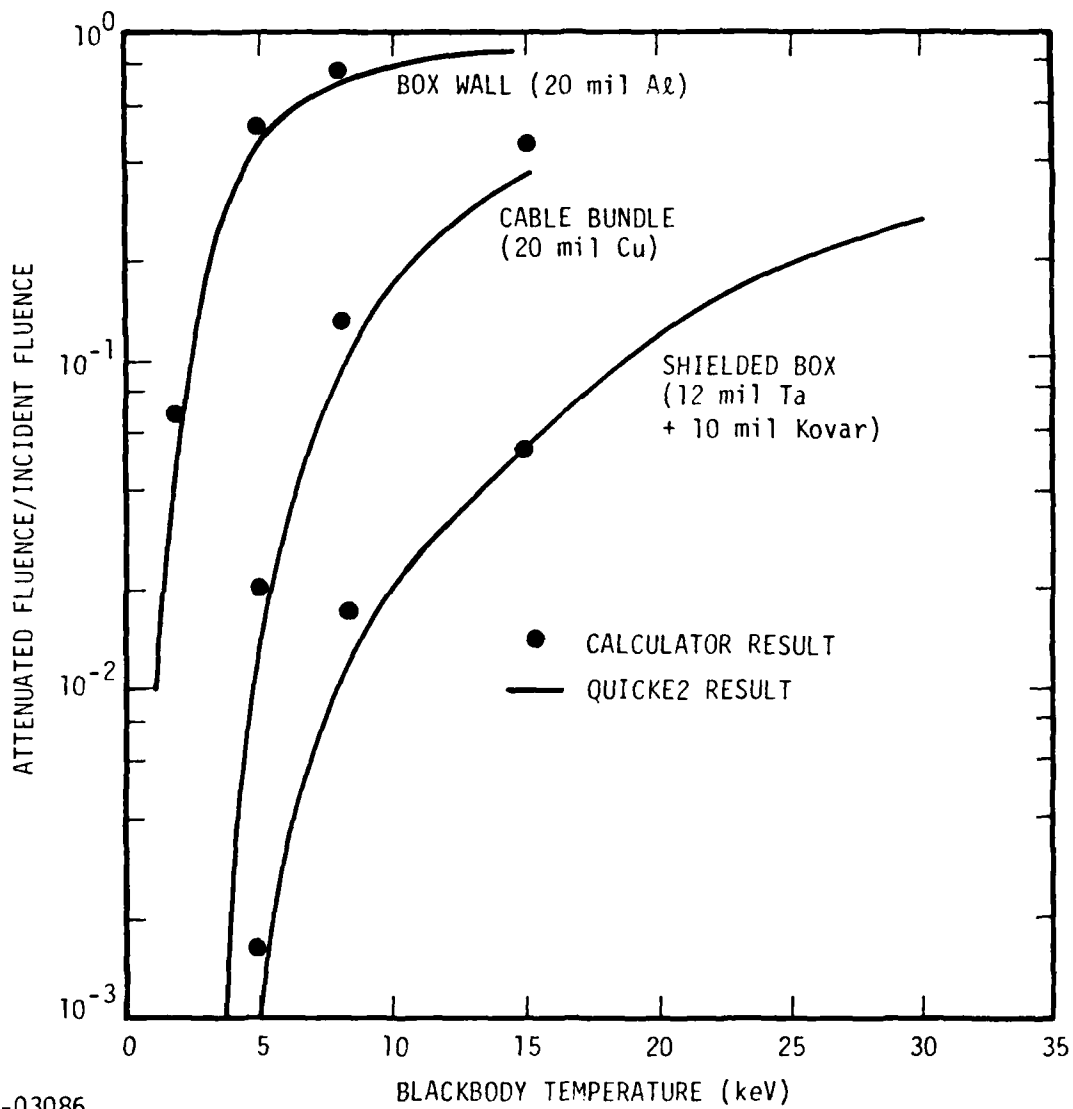
Figure 6. X-ray shinethrough fraction calculated with TI-59 attenuation program, compared to QUICKE2 code results for representative satellite materials

RE-03086

Comparisons between the calculator and the multidimensional code results are shown in Figures 7 and 8. The graphs are presented in scaled format (Ref. 8) involving the products, ΦR ("fluence product"), $E_z R$ ("electric field product"), and normalized incident pulse time history, $\Delta T / 2\pi R/c$, where ΔT is the x-ray pulse width and $2\pi R/c$ is the time required for an electromagnetic wave to traverse the circumference of the cylinder.

Figure 7 shows the effects of varying the incident pulse width for a constant spectrum at different fluence levels, and Figure 8 shows the effects of varying the incident fluence for different x-ray spectra. (Figure 1 shows the effect of varying the incident spectrum temperature at constant pulse width for different fluences.) This scaled format extends the applicability of the results to a wide range of object sizes. As an example of the use of the scaled quantities indicated in the figures, Figure 7 can be used to estimate the peak response of a 2-m-radius object when excited by a 200-nsec photon pulse at a fluence of 5×10^{-3} cal/m^2. For $R = 2$ m, the 5×10^{-3} cal/m^2 isofluence line corresponds to the bottom curve in the figures. For 100 nsec and $R = 2$ m, the abscissa is $(10^{-7}$ sec) $\times (3 \times 10^8$ m/sec)$/(2\pi \times 2$ m), or 2.39. The corresponding total current on the object is about 0.5 amps. The magnetic field is $1/2\pi R$, or 4×10^{-2} amp/m.

Agreement between the calculator and the 2-D code results is seen to be excellent in the space-charge-limited regimes, as well as in the non-space-charge-limited regimes which involve relatively short pulse lengths compared to object dimensions. The agreement begins to deteriorate particularly for low-fluence, long-pulse-length problems (notice the lower right-hand portion of Figure 7) due to limitations of the present modeling when the electron cloud extent becomes comparable to object dimensions. This limitation is discussed in Reference 9 in relation to large-scale calculations. By virtue of the scaled format, the inaccurate region of the parameter range can be seen to become greater as the object size is decreased.

Overall accuracy of the system can be described as excellent for the external SGEMP problem, however. Errors remaining can be reduced significantly with moderate improvements in the modeling.

5.3   CAVITY RESPONSE

The internal response of a cylindrical cavity has been quantified with the calculator codes and compared against ABORC results. The cavity is a 1-m length=diameter empty cylinder with 3-mil aluminum walls, and is representative of the larger empty volumes found in satellites. Moderate attenuation of x rays caused by the thin walls

22

QUICKE2 EXCITATION
PARAMETERS

$YIELD = 1.2 \times 10^{-6}$ C/cal

$\bar{v}_Z = 2.1 \times 10^7$ m/sec
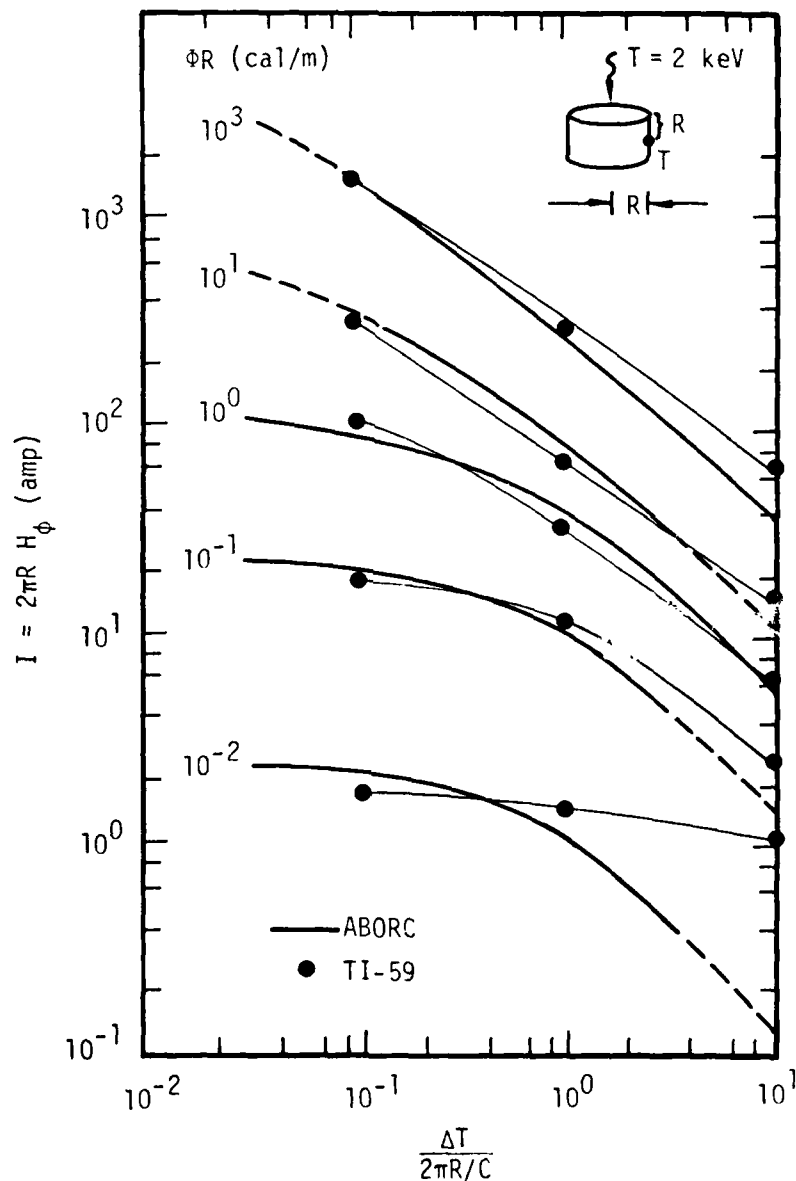
RE-03191

Figure 7. Peak surface current versus characteristic pulse time
for various fluence products using a 2-keV blackbody spectrum.
Fluence products ΦR in cal/m are noted by each curve.
The x-ray pulse rise time was ≈ 0.6 × Δt.
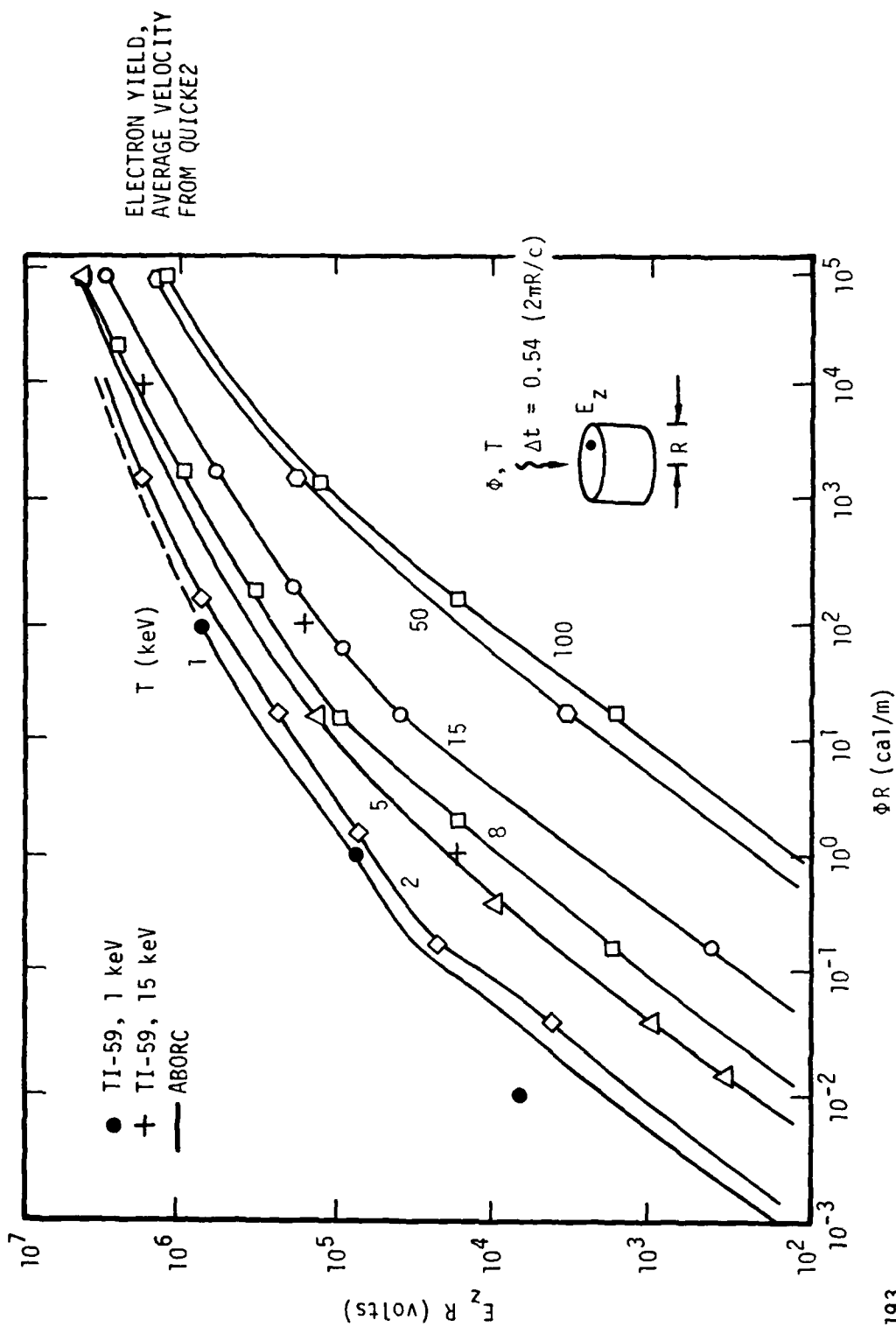
23

Figure 8. Peak electric field product versus fluence product for various spectrum temperatures. Solutions apply for an incident pulse width $\Delta t = 0.54(2\pi R/c)$, where c is the speed of light. The x-ray pulse rise time was $\approx 0.6 \times \Delta t$.

RE-03193

24

results in significant signals inside. Moderate space-charge-limiting occurs at the assumed fluence level of 10^{-3} cal/cm^2. The incident spectrum is a 5-keV blackbody with rise time and pulse width (FWHM) of 10 and 17 nsec, respectively.

Results from the two methods of calculation are compared in Figure 9. The TI-59 excitation parameters (I_e and $\langle v \rangle$) agree very well with results from the QUICKE2 code, mainly because differences should be due to energy bin limitation only. The electromagnetic field peak values are less accurate due to geometry problems. The calculator results are three to five times higher than the more exact ABORC values due to present limitations of the simple models for this case. In the test problem, the electrons can traverse the entire cavity during the pulse width of the x rays, whereas the analytical models are exact only for cases in which the electron cloud is small compared to object dimensions. Other geometry effects contribute to errors, including cylinder aspect ratio and electron angular distributions. The agreement between the calculations is sufficient for problem scoping, however (notice the calculator gives upper-bound values), and variations of input parameters would tend to give reasonably accurate assessment of tradeoffs in designing for hardening.

The comparison problem shown here points out the limitations of the present solutions for small internal cavities and low fluence levels. Increasing the fluence would result in improved correlation of the parameter values between ABORC and the calculator by reducing the space-charge cloud dimensions relative to the cavity size. Similarly, a decreased x-ray pulse width would result in greater accuracy.

5.4   BOX CURRENTS

The calculator codes have been applied to analysis of SGEMP effects on a printed circuit (PC) board inside a typical satellite electronics equipment box (see Figure 10). Worst-case estimates were obtained of SGEMP currents flowing on individual grounded lands on the fiberglass board for a given x-ray environment. Normally, such an analysis might be conducted with simple analytical estimates once the photon attenuation and excitation parameters were established, with some degree of accuracy, by a computer calculation. The results shown in the figure can be obtained in about 10 minutes with the calculator, with the analyst having to press only a few buttons rather than having to know many different formulas. Parameter variations for hardening measures or arbitrary spectra can be conducted on the box configuration with ease, also.

1 m

E

1 m

3 mils Aℓ ⟶

H

T = 5 keV

T_R, ΔT = 10, 17 nsec

$\Phi = 10^{-3}$ cal/cm^2
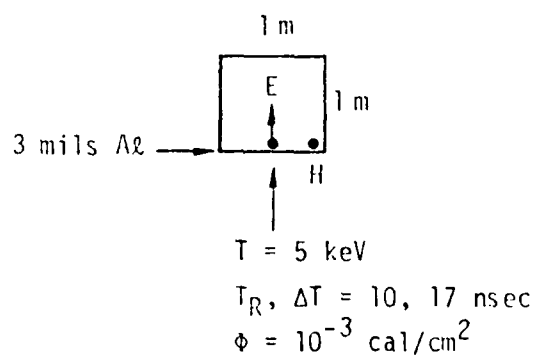
PARAMETER	QUICKE2/ABORC	CALCULATOR
ELECTRON VELOCITY, v (m/sec)	3.3×10^7	3.3×10^7
ELECTRON YIELD, Y (C/cal)	1.8×10^{-7}	2.3×10^{-7}
EMISSION CURRENT, J_e (amp/m^2)	100	135
ELECTRIC FIELD RATE, $\dot{E}$ (V/m/sec)	3.5×10^{12}	1.5×10^{13}
PEAK ELECTRIC FIELD, E (V/m)	3.8×10^4	1.1×10^5
MAGNETIC FIELD RATE, $\dot{H}$ (amp/m/sec)	9.2×10^8	3.8×10^9
PEAK MAGNETIC FIELD, H (amp/m)	12	34

Figure 9. Comparison of calculator code results with
QUICKE2/ABORC results for internal cavity analysis

X-RAY ENVIRONMENT

BB TEMPERATURE, T = 5 keV

FLUENCE, $\phi = 10^{-1}$ cal/cm^2

RISE TIME, $t_R = \Delta t = 10^{-8}$ sec

ELECTRON YIELD, $Y = 1.0 \times 10^{-8}$ C/cal

$J_e = 4.0 \times 10^3$ amp/m^2

$\bar{v} = 4.0 \times 10^7$ m/sec

In figure (labels):

10 cm

10 cm

2 cm

FIBERGLASS PRINTED CIRCUIT BOARD, CONFORMAL COATING (LOW-Z), 0.2-cm-THICK LANDS, $\ell = 10$ cm, GROUNDED THROUGH LOW IMPEDANCE, COVERING 5% BOARD AREA

(WORST-CASE KNOCK-ON, CV)

(WORST-CASE $\dot{B}A$ EXPOSURE)

40 mils Aℓ
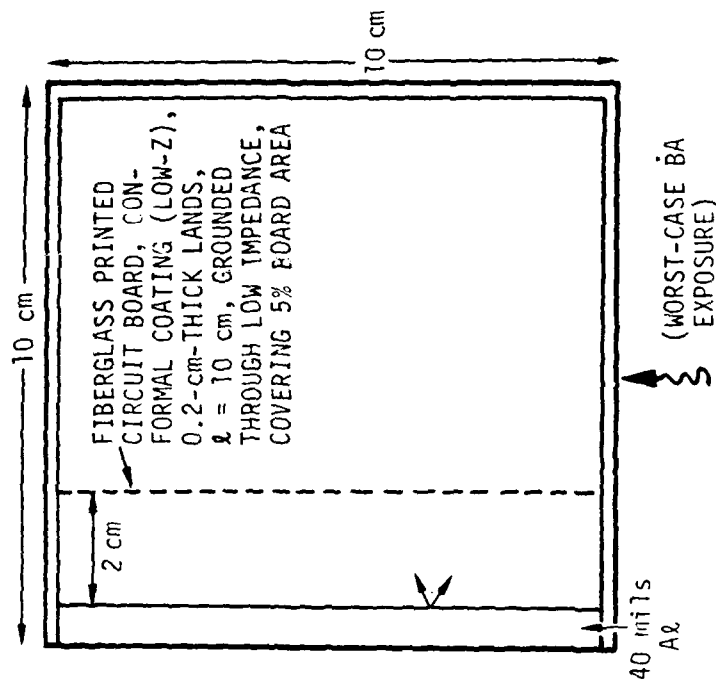
WORST-CASE CURRENTS FOR ALL ORIENTATIONS (amp)

KNOCK-ON	CV	$\dot{B}A$
1.6	6.3	3.4

RE-03194

Figure 10. Example box analysis results obtained with the calculator programs. The worst-case knock-on and CV currents occur due to x rays incident from the left, and the worst-case $\dot{B}A$ is caused by illumination from the bottom, as shown.

27

6. SUMMARY OF CAPABILITIES ON THE CALCULATOR

A summary of SGEMP phenomenology capabilities on the TI-59 is shown in Table 3. The parameter ranges for which the models were specifically developed are indicated. The codes can be applied outside the indicated ranges (except for the energy range), but the user must be careful to interpret the results properly. For example, mass absorpton of x rays due to more than 15 mils of tantalum can become very delicate with only 14 energy bins, and answers may be very much dependent on the particular energy bins selected. Attempts to quantify overall accuracy of the system for SGEMP effects within the designated ranges are made, as shown in the column labeled "Accuracy."

Table 3. Summary of SGEMP Phenomenology Capabilities on the TI-59

Parameter Ranges: Satellite locations
X-ray energies from 1 to 1000 keV
X-ray fluence up to 10^{-1} cal/cm^2
X-ray pulse widths from 2 to 200 nsec

Calculation	Accuracy	Principal Caveats
X-ray attenuation	Within factor of 2 of QUICKE for SGEMP spectra	Energy bins must be selected intelligently
		Compton effects ignored
		Exercized only for representative materials to date
Photoemission excitation parameters	Within factor of 2 of QUICKE	Energy bin selection
E&M response parameters	Within factor of 4 of ABORC	Low-fluence, long-pulse-length geometry effects not treated accurately (includes most box effects)
	Calculator results are upper bounds	Moderate space-charge-limiting and angular effects in cavities not treated
Cable coupling	Accuracy not tested but calculator techniques are commonly used in analyses with present degree of accuracy	Direct-drive estimate crude
		Knock-on current not self-consistent

Notice from the table that factor-of-2 accuracy can be achieved with intelligent energy bin selection for the first two categories of calculations. This is sufficiently accurate for scoping of effects. Determination of electromagnetic response parameters is a little less certain, but the calculator gives upper bounds on results in every case. Major problems are in the regimes of low fluence and small dimensions and can be corrected with simple analytical estimates by the experienced analyst.

Cable coupling estimates are accurate for cable lengths short compared to x-ray pulse lengths. The direct-drive model is presently limited to a simple estimate based on the dipole moment from a planar surface. Accuracy of this model has not been compared with more detailed calculations, but better than an order of magnitude is expected from it. The knock-on current onto a cable shield does not take into account the effect of the cable itself on fields in a cavity, so this driver can be low by large amounts, especially for low-impedance cables at high fluence.

In general, the accuracy for the first three categories in Table 3 is such that analytical estimates of effects can be upgraded considerably through use of the system compared to present quick-response analysis methods. The system handles the most sensitive and time-consuming calculational areas with the greatest accuracy, and areas of weakness can be compensated for through relatively simple considerations. For example, inaccuracy at low fluence inside a cavity will likely be as great due to complex cavity geometry effects not treated in that case as due to modeling assumptions used here.

REFERENCES

1. A. J. Woods and E. P. Wenaas, "Photon Source SGEMP Spectrum Evaluations," DNA 5261F, April 1978.

2. A. J. Woods and E. P. Wenaas, "SGEMP Geometry Effects," IEEE Trans. Nucl. Sci. NS-22, No. 6, December 1975.

3. F. Biggs and R. Lighthill, "Analytical Approximations of X-Ray Cross Sections II," SC-RR-71-0507, December 1971.

4. T. A. Dellin and R. E. Huddleston, "Second-Generation Analytical Photo-Compton Current Methods," IEEE Trans. Nucl. Sci. NS-22, No. 6, December 1975.

5. N. J. Carron and C. J. Longmire, "On the Structure of the Steady-State Space-Charge Limited Boundary Layer in One Dimension," DNAn 3928T, November 1975.

6. A. Wilson and D. E. Parks, IEEE Trans. Nucl. Sci. NS-23, No. 6, December 1976, p. 1916.

7. A. J. Woods and T. N. Delmer, "The Arbitrary Body-of-Revolution Code (ABORC) for SGEMP/IEMP," DNA 4348T, July 1976.

8. A. J. Woods and E. P. Wenaas, "Scaling Laws for SGEMP," IEEE Trans. Nucl. Sci. NS-23, No. 6, December 1976.

9. R. G. Stettner, "On the Limits of Applicability of the Space-Charge-Limited $\dot{P}$ Driver," DNA 4630T, June 1978.

APPENDIX A

DETAILS OF SGEMP MODELING
FOR THE PROGRAMMABLE CALCULATOR

This appendix contains details of the modeling used in the four divisions of SGEMP calculations treated here. Section A.1 describes the photon attenuation, A.2 the excitation parameters, A.3 the electromagnetic response parameters, and A.4 cable coupling. The physics and modeling for each category are described and compared against more exact calculations.

A.1   X-RAY ATTENUATION

Analytical expressions for cross sections have previously been developed (Ref. A-1) and are the basis for x-ray attenuations in standard photon energy deposition/electron emission codes (Ref. A-2). The expressions employ summations of inverse powers of photon energy in the photoelectric regime, where the coefficients are based on least-square fits to available experimental and detailed calculational data. The present work simply reduces the method even further to a general approach suitable to rapid and convenient use on a programmable calculator. Limited storage capability prevents expeditious handling of large data bases, and some degree of inaccuracy is necessarily introduced. The simplified method and degree of accuracy are discussed below.

An expression which can reasonably approximate the photoelectric absorption coefficient in the energy range $\mathcal{E} = 1$ to 1000 keV is

$$\kappa(\mathcal{E}) = \frac{\kappa_u(\gamma, \xi)}{Z^3} \quad (cm^2/g) , \tag{A-1}$$

where Z is the atomic number of the material and κ_u is the universal function:

$$\kappa_u = \sum_{i=1}^{4} \frac{B_i H(\gamma - \gamma_{0i})}{\xi^3} , \tag{A-2}$$

$$\xi = \mathcal{E}/Z^2 , \quad \gamma = \mathcal{E}/Z^{2.24} . \tag{A-3}$$

B_i is a constant coefficient for an energy level (see Table A-1), $H(x)$ is the step function, and $\gamma_{0i} = \mathcal{E}_{0i}/Z^{2.24}$ where $\mathcal{E}_{0i}$ is approximately the energy of the ith absorption edge of a material.

31

Table A-1. Universal Attenuation Function Coefficients
and Cutoff Energies

| Edge | i | $Z < 29$ | | $Z > 29$ | |
		β_i (cm^2/g)	γ_{0i} β_i (keV·cm^2/g)	γ_{0i} (keV)	
k	1	8.6	4.8×10^{-3}	12.6	4.5×10^{-3}
ℓ	2	0.82	4.8×10^{-4}	1.25	6.7×10^{-4}
m	3	0.13	1.2×10^{-4}	0.14	1.2×10^{-4}
n	4	0.035	3.3×10^{-5}	0.010	1.9×10^{-5}

It is important to remember that only photoelectric absorption is included in the expression. Auger absorption (low energies) and Compton scattering (high energies) are not treated. These effects tend to be unimportant for SGEMP in the energy range considered here and so are not included.

A comparison of the universal attenuation coefficient with more exact curves is shown in Figure A-1 for several elements with a wide range of atomic numbers. Greatest errors occur for high-Z materials (see gold). In general, the absorption is approximated to within a factor of 2 of the more exact curves until Compton scattering becomes dominant (at high energies). The approximate treatment has not been compared with the more accurate curves for every element, but accuracies similar to those exhibited are expected for other cases.

The approximate method appears to give photon attenuations that are suitable for the present work. Errors introduced will tend to be smoothed out for most spectra due to integration over energy for most SGEMP effects. Caution is recommended in using monoenergetic spectra with this method, since worst-case errors would occur with them.

The capacity of the simplified approach to handle all elements with a single algebraic formula and a small data base makes it ideal for use in a programmable calculator. Additionally, the coefficients of Table A-1 can be changed easily for more accurate fits for a given element. Those shown are chosen to represent all elements without being changed between calculations.

It should be noted that the agreements shown in Figure A-1 were obtained with coefficients in the attenuation expression which are material-dependent. At present, the calculator program employs a data card for low-Z ($Z < 29$) materials and a second card for
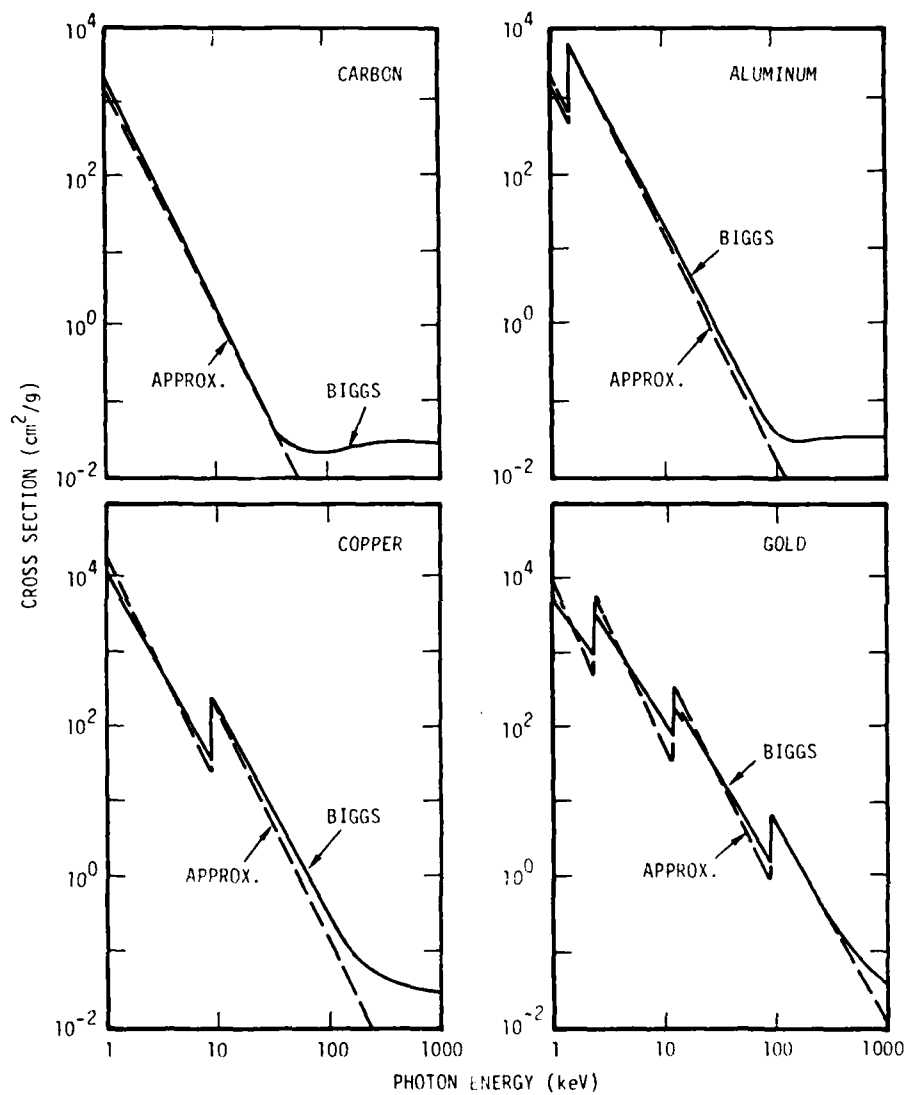
Figure A-1. X-ray photoelectric absorption cross sections obtained
using a single expression for all elements. The energy-absorption
cross sections of Biggs and Lighthill (Ref. 1) are shown for comparison.

RE-03184

33

high-Z materials. Original plans for a single set of coefficients for all materials were implemented, but considerably better acuracy was realized when attenuation data for ranges of material were fit more exactly.

The attenuation program is also capable of treating multiple plates through repeated application, employing the output spectrum from one plate as the input spectrum to the next. Compounds are calculated by breaking the elements into separate plates according to their mass ratios.

A.2 EXCITATION PARAMETERS

Excitation parameter calculations are required for the electric yield, average velocity, and dipole moment for electron spectra emitted into cable dielectrics. A data base for these quantities has been developed for representatives of the full range of satellite materials (carbon through gold), including a few composites (SiO_2, Mylar, fiberglass). Values for the excitation parameters were calculated and tabulated as a function of monoenergetic x-ray energy using the QUICKE2 photoelectron emission computer code. The results for x-ray spectra are obtained by convolving the monoenergetic values with properly attenuated photon spectra using appropriate algorithms (Ref. A-3).

The accuracy of the data base employed in the calculator codes is essentially the same as that of the QUICKE2 code itself. The latter has been shown to provide factor-of-2 agreement with experimental data and detailed Monte Carlo calculations for wide ranges of photon and material parameters (Ref. A-4), and is generally considered the industry standard for SGEMP analyses. Some inaccuracies in interpolating the data base values over the range from 1 to 1000 keV occur because the calculator programs permit a maximum of 14 energy bins. The accuracy of the excitation parameters is usually within a factor of 2 of QUICKE2 calculations for the same spectrum, however, because power-law fits to the data base are employed.

Figure A-2 shows a comparison of results for excitation parameters obtained with the calculator codes and with QUICKE2 for blackbody spectra. The agreement is considerably better than factor-of-2 over a wide energy range. Errors due to inexact curve-fitting at different energies may be averaged out for a spectrum of x rays. The TI-59 results employed 14 energy bins for photons, while QUICKE2 results were obtained using 50 bins. Appendix C contains details of the data base parameters.
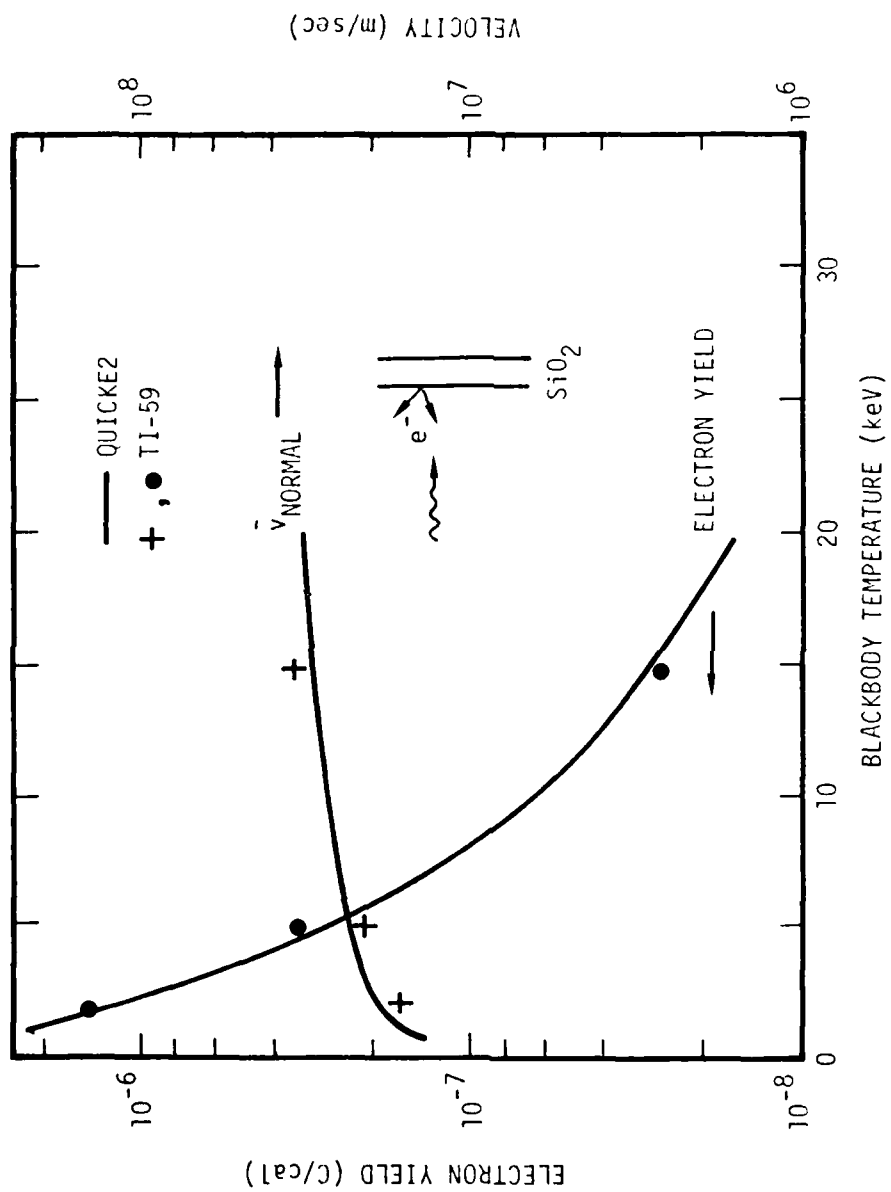
34

Figure A-2. Example excitation parameters for external emission from quartz obtained with the TI-59 data base compared to the QUICKE2 electron emission code

RE-03190

A.3   ELECTROMAGNETIC RESPONSE PARAMETERS

A simple analytical formulation is derived for estimating the maximum rates of change of the space-charge dipole moment ($\dot{P}$) and the surface electric field ($\dot{E}$) for an SGEMP excitation of an infinite plane in free space. The quantities $\dot{P}$ and $\dot{E}$ for a planar geometry are useful parameters for comparing the relative SGEMP exterior responses of real systems due to excitation pulses with different pulse shapes, fluences, and electron emission yields and energies. For an emission pulse whose intensity increases linearly from zero to a maximum at time t_1 and is then constant for the remaining time of interest, the peak values of $\dot{P}$ and $\dot{E}$ and the times of their occurrence can be calculated by simple mathematical expressions which can be readily incorporated into a programmable calculator.

An expression for the peak electric field at the surface of a photon-illuminated plate is also described. Although this field is not particularly useful for estimating SGEMP responses, which are primarily functions of $\dot{B}$ and $\dot{E}$, it is a convenient quantity for illustrating the intensity of the photon pulse.

A.3.1   Foreword

There are two dominant mechanisms for coupling the SGEMP fields into an electronics system. One is $C\dot{V}$, where C is the capacitance between a cable and a nearby conducting surface of the system and $\dot{V}$ is the rate of change of the voltage between the cable and the wall. For a fixed geometry, $C\dot{V}$ is proportional to $\dot{E}$, where E is the average electric field between the cable and the wall. Since the largest E fields on an SGEMP-excited body usually occur just above the illuminated surface, a one-dimensional planar calculation of $\dot{E}$ adjacent to the illuminated surface should be a measure of the worst $C\dot{V}$ coupling that could result from the photon pulse and target material under investigation.

The other coupling mechanism is the $\dot{B}$ coupling into the circuit due to the magnetic fields associated with the SGEMP structural return currents. In Reference A-5, it was shown that the structural return currents (and, hence, the surface H fields) at a point on the outside of a body that is not too close to the illuminated area of the body are reasonably proportional to $\dot{P}$, the rate of change of the space-charge dipole moment at the illuminated surface. Thus, the peak value of $\dot{P}$ and its time derivative $\ddot{P}$ provide useful measures of the relative $\dot{B}$ coupling for a system that is exposed to different photon pulses. A minor, but sometimes useful, additional application of the time to the

peak $\dot{P}$ is a guide for choosing suitable time steps for more detailed computer calculations.

In Section A.3.2, the basic model used in this report to estimate the peak $\dot{P}$ and $\dot{E}$ is described, and the general mathematical equations for an arbitrary emission current time history $[J_{em}(t)]$ are derived. These equations are then integrated for a trapezoidal emission time history. When the peak $\dot{P}$ occurs in the linearly increasing or constant regions of the trapezoidal pulse, the peak magnitude of $\dot{P}$ and the time of its occurrence can be obtained in simple mathematical closed forms. Also, a simple algorithm gives an approximate value for the peak $\dot{E}$.

In Section A.3.3, a comparison is given of results from these simple formulas with results from a one-dimensional particle-pushing code which uses a distribution of electron emission energies.

A.3.2   Description of the Model

In a one-dimensional planar problem with the other boundary at infinity (an open-circuit diode), the electric field at the emitting surface (E) is just $1/\varepsilon$ times the total charge densty per unit area (Q) that has been emitted from the surface and has not yet returned to it. Early in the pulse, before any charge has returned to the surface,

$$E(t) = \frac{1}{\varepsilon} \int_0^t J_{em}(t') \, dt \; . \tag{A-4}$$

Thus, particles that are emitted at time t initially feel this electric field. Moreover, until these particles overtake some particles that were emitted at an earlier time, or until some later-emitted particles overtake those emitted at time t, it is rigorously correct that these particles will continue to feel the same constant field E(t). For the times of interest for this analysis, it is assumed that all emitted particles continue to experience the magnitude of the E field into which they were first emitted [E(t)], even though some spatial mixing of the particles does occur. (This is the "gravitational" approximation used in Reference A-6 to develop a thin boundary layer SGEMP driver for a finite-difference code.)

The next assumption of this model is that all of the emitted electrons have the same initial velocity normal to the emission surface (v_{ave}). It turns out that these two approximations give quite good results up to the time of the peak $\dot{P}$ and fairly good results up to the peak $\dot{E}$ as ong as the energy spectrum of the emitted electrons is not too broad with a long range of emission velocities. With the above approximations, the equation for $\dot{P}(t)$ is

37

$$\dot{P}(t) = \int_0^t \left[v_{ave} - E(t') \frac{e}{m} (t-t') \right] J_{em}(t') \, dt' \, , \tag{A-5}$$

where e is the absolute value of the electronic charge and m is the mass of the electron. In Eq. A-5, the term in the large brackets is the velocity at the time t of the electrons that were emitted at time t' into the constant electric field $E(t')$.

A.3.3   Expression for $\dot{P}$

For an emission current $J_{em}(t)$ that increases linearly from zero to a value of J_m at $t = t_1$,

$$\dot{P}(t) = J_m \left(v_{ave} \frac{t^2}{2t_1} - \frac{e \, J_m \, t^5}{\varepsilon \, m \, 40 \, t_1^2} \right) . \tag{A-6}$$

If $\dot{P}$ reaches a maximum before t_1, the maximum will occur at

$$t_{m1} = \left(\frac{8 v_{ave} \, \varepsilon \, t_1}{J_m \, (e/m)} \right)^{1/3} , \tag{A-7}$$

and the peak value of $\dot{P}$ can be obtained by substituting t_{m1} in place of t in Eq. A-6.

For small values of J_m, the value of t_{m1}, as calculated by Eq. A-7, can be greater than t_1, so the maximum in $\dot{P}$ occurs after t_1. The equation for $\dot{P}(t)$ during the constant part of the trapezoidal emission pulse is

$$\dot{P}(t) = J_m \left[v_{ave} \frac{t_1}{2} - \frac{J_m \, e}{\varepsilon m} \left(\frac{1}{2t_1^2} \right) \left(\frac{t \, t_1^4}{4} - \frac{t_1^5}{5} \right) \right] + J_m \left[v_{ave}(t-t_1) - \frac{J_m \, e}{\varepsilon m} \right.$$

$$\left. \left\{ \frac{t}{2} \left(t^2 - t_1^2 \right) - \frac{t \, t_1}{2} (t-t_1) - \frac{(t^3 - t_1^3)}{3} + \frac{t_1}{4} \left(t^2 - t_1^2 \right) \right\} \right] . \tag{A-8}$$

The terms in the first square bracket are the contribution to $\dot{P}$ from the electrons emitted before t_1, and those in the second square bracket are the contribution from the electrons emitted after t_1 (during the constant portion of the emission pulse).

The maximum value of Eq. A-8 occurs at

$$t_{m2} \approx \frac{t_1}{2} + \left(\frac{2 v_{ave} \, \varepsilon m}{e \, J_m} \right)^{1/2} , \tag{A-9}$$

and the maximum value of $\dot{P}$ is obtained by substituting t_{m2} for t in Eq. A-8.

For very small values of J_m with a given pulse width, the peak value of $\dot{P}$ will occur after the constant portion of the trapezoidal pulse. It is possible to obtain an expression for $\dot{P}$ during the linearly decreasing leg of the trapezoidal pulse. However, the resulting equation for the time when $\dot{P}$ is maximum is fourth-degree and would have to be solved by iteration. Even though an iteration is relatively simple on a large computer, the storage requirements would probably exceed the capabilities of present-day simple programmable calculators. Fortunately, if the peak $\dot{P}$ occurs after t_1, one would make only a minor error if one assumed that the emission pulse were constant out to the halfway point on the linearly decreasing portion of J_{em} and used Eqs. A-9 and A-8 to obtain the time of occurrence and the magnitude of the peak $\dot{P}$.

A.3.4   Expression for $\ddot{P}$

The simplest way of getting $\ddot{P}(t)$ is just to differentiate $\dot{P}(t)$. For $t < t_1$,

$$\ddot{P}(t) = J_m \left(v_{ave} \frac{t}{t_1} - \frac{e}{\epsilon} \frac{J_m}{m} \frac{t^4}{8t_1^2} \right).$$ (A-10)

Equation A-10 has a maximum at

$$t = \left(2 \frac{v_{ave}}{J_m} \frac{t_1 \epsilon}{(e/m)} \right)^{1/3}.$$ (A-11)

If this t is less than t_1,

$$\ddot{P}_{max} = \frac{J_m}{4} \frac{v_{ave}}{t_1} \left(2 \frac{v_{ave}}{J_m} \frac{t_1 \epsilon}{(e/m)} \right)^{1/3}.$$ (A-12)

For $t_1 < t < t_2$,

$$\ddot{P}(t) = J_m \left[\frac{-J_m e}{\epsilon m} \frac{t_1^2}{8} + v_{ave} - \frac{J_m e}{\epsilon m} \left(\frac{t^2}{2} - \frac{t t_1}{2} \right) \right].$$ (A-13)

The first two terms in Eq. A-13 (the constant terms) are the value of $\ddot{P}(t)$ at $t = t_1$. The last term is always subtractive so the peak of $\ddot{P}(t)$ occurs at $t = t_1$.

Therefore, for $\ddot{P}_{max}$, calculate t from Eq. A-11. If this t is less than t_1, substitute into Eq. A-10 or Eq. A-12 to get $\ddot{P}_{max}$. If that t is greater than t_1, evaluate $\ddot{P}_{max}$ from Eq. A-10 with $t = t_1$.

39

A.3.5 Expression for $\dot{E}$

By differentiating Eq. A-4 with respect to time, one obtains

$$\dot{E}(t) = \frac{1}{\varepsilon} J_{em}(t) \; ; \tag{A-14}$$

that is, $\dot{E}(t)$ is directly proportional to the emission current up to the time that any emitted electrons return to the emission surface. If this time for the first electrons to return is greater than t_1 (that is, the time when J_{em} first reaches its peak value of J_m), the peak value of $\dot{E}$ is obviously

$$\dot{E}_m = \frac{1}{\varepsilon} J_m \; . \tag{A-15}$$

If the first electrons return to the emitting surface before t_1, the curve of $\dot{E}(t)$ will start to drop below the linear curve of $[(1/\varepsilon) J_{em}(t)]$ and then reach a maximum value. Unfortunately, the present model cannot be used to obtain a rigorous value for the peak $\dot{E}$ because the peak $\dot{E}$ occurs after considerable spatial mixing has occurred between electrons emitted at different times. Consequently, several different algorithms were tried with the present model to find an approximate method of estimating a conservatively large value of the peak $\dot{E}$.

A relatively simple approach that gives somewhat conservative (large) values for the peak $\dot{E}$ is to assume that the peak $\dot{E}$ occurs when $\dot{P}$ returns to zero. From Eq. A-6, $\dot{P}$ returns to zero at

$$t_{m3} = \left(\frac{20 v_{ave} \, e \, t_1}{J_m \, (e/m)} \right)^{1/3} \; . \tag{A-16}$$

Thus, by the present assumption, the peak $\dot{E}$ would be given by

$$\dot{E}_{max} = \frac{1}{\varepsilon} J_{em}(t_{m3}) \; . \tag{A-17}$$

The main rationale for this approach is that it gives reasonably good comparison with results from a one-dimensional particle-pushing code, as shown in Section A.3.7. However, a plausibility argument is that the dipole moment P is maximum when $\dot{P} = 0$. Thus, on the average, the emitted electrons are at the maximum distance from the emitting surface. Thereafter, the emitted particles will return very rapidly to the emitting surface and prevent $\dot{E}$ from increasing significantly more.

A.3.6   Quasi-Static Approximation for E in the Space-Charge Region

The general formula for the peak steady-state E, from Reference A-7, is (in MKS units):

$$E_m = \sqrt{Fmr_0}\ v_1/\varepsilon\ ,\qquad\qquad (A-18)$$

where F is a dimensionless number that is a function of the emission spectrum and angular distribution, m = electron mass, r_0 = electron emission rate = J_e/e, v_1 is the characteristic velocity of the electron spectrum, and ε is the permittivity of free space. Reference A-7 evaluates F for four rather different spectra, as summarized in Table A-3.

Fortunately, the F terms differ by, at most, a factor of 1.7 for these four energy distributions. Thus, the maximum steady-state E fields should differ by at most $\sqrt{1.7} \approx$ 1.3. If one just considers the $\cos\theta$ distributions (cases 2, 3, and 4), the F terms differ by only 1.5 and the E terms by $\sqrt{1.5} \approx 1.22$. For average results, one can use F = 3.0. Also, for a $\cos\theta$ distribution, $v_1 = \sqrt{2}\ v_{normal}$.

Table A-3. Parameters Describing Analytical Electron Energy Spectra
and Resultant Space-Charge-Limiting of Electric Fields

Case	1	2	3	4
Description	Monoenergetic (energy = w_1) normal to emission plate	Monoenergetic (energy = w_1) $\cos\theta$ angular distribution	Linear times exponential energy distribution, $\cos\theta$ angular distribution	Exponential energy distribution, $\cos\theta$ angular distribution
dn/dw	Delta function at $w_1[=r_0\delta(w-w_1)]$	$r_0\delta(w-w_1)$	$\dfrac{r_0 w}{w_1^2}\exp(-w/w_1)$	$\dfrac{r_0}{w_1}\exp(-w/w_1)$
F	4	$8/3 = 2.67$	$2\pi^{1/2} = 3.54$	$4\pi^{1/2}/3 = 2.36$

Figure A-3 shows calculated time histories of E using a one-dimensional particle-pushing code for an electron spectrum with an average $v_{normal} = 3.54 \times 10^7$ m/sec and a trapezoidal emission pulse (10-nsec rise time), with four values of peak emission rate. The asymptotic values of the dynamic calculations agree remarkably well (perhaps partly fortuitously) with the analytical steady-state values, considering that the value of F = 3.0 which was used is just an average. Anyway, the asymptotic values scale as $\sqrt{J_e}$, as the analytical expression predicts.

Several other calculations using different emission spectra and emission rates showed comparable agreement, always using F = 3.0.

In conclusion, it appears that one is well justified in using the steady-state formula (Eq. A-18) for the peak E with an average F = 3.0. If the pulse length is less than the space-charge plasma period, this procedure overestimates the peak E. For example, if the 10^5 amp/m^2 pulse had ended at 4 nsec, where the dynamic calculations stopped, the analytic formula would have predicted $E = \sqrt{0.4} \times 3.1 \times 10^7 = 1.96 \times 10^7$ V/m, compared to the dynamic value of 1.85×10^7 V/m. Also, the expression does not apply in the non-space-charge-limited regime.

A.3.7 Comparison to Results from 1-D Particle-Pushing Code

The one-dimensional particle-pushing code used for comparison to the above simple model emits an arbitrary (input) number of particles per time step with a distribution of normal velocities. The total charge emitted per time step is proportional to the instantaneous emission current, and is distributed among the emitted particles consistent with an arbitrary (input) electron emission energy spectrum.

Results from this code for various trapezoidal emission pulses and peak emission currents are compared in Table A-4 to results from the present simplified model. The electron energy spectra used in the particle-pushing code covered the range from zero up to 130 keV, with the maxima occurring at from 1 to 5 keV. As can be seen from Table A-4, the values for the peak $\dot{P}$ as calculated by the simplified model are in quite good agreement with the results from the particle-pushing code (within about 10%).

It is interesting that the first ten problems shown in Table A-4 used an early version of the particle-pushing code which did not distribute the emission particles below 1 keV because that was as low as the QUICKE2-generated emission spectra extended. Thus, the velocities of the emission particles were grouped relatively closely around the average electron velocity. The outcome is that the $\dot{P}$ results from the simplified model agree almost exactly with the particle-pushing results, as one would expect. For the later
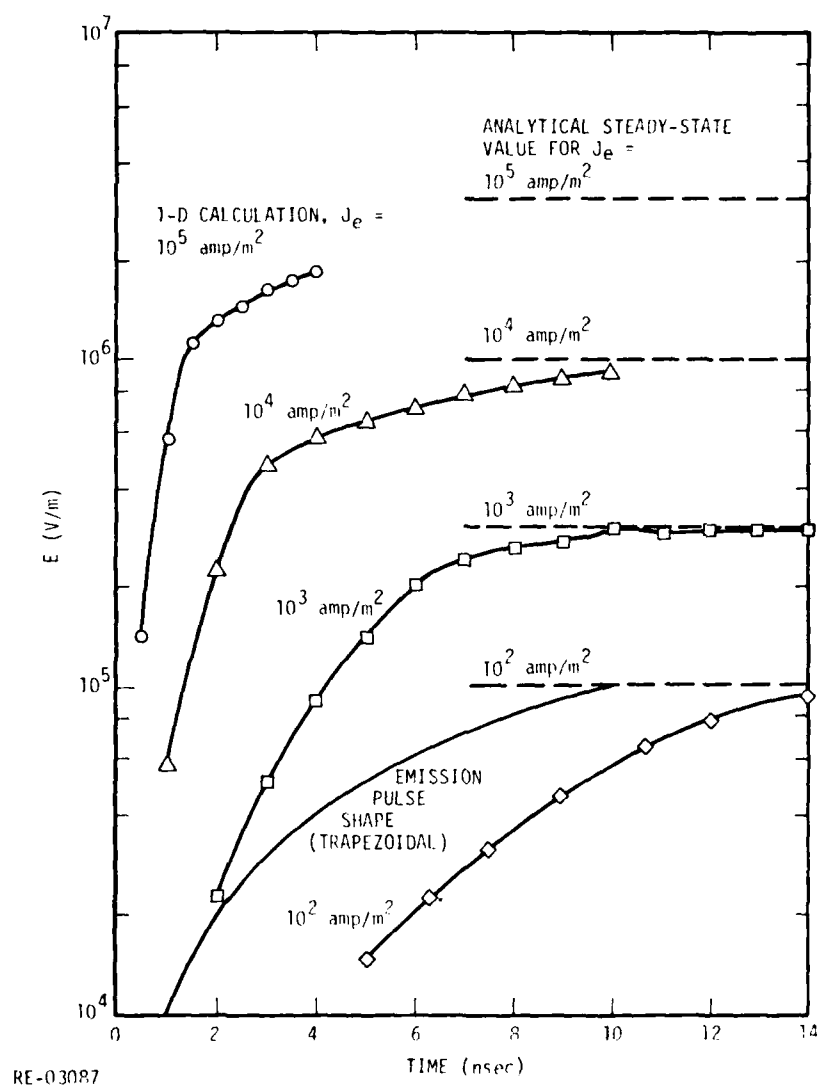
Figure A-3. Electric field at emission surface; 1-D dynamic
particle-pushing calculation and steady-state analytical results

RE-03087

Table A-4. Comparison of Peak $\dot{P}$ and $\dot{E}$ from Simplified Model and Particle-Pushing Code

Pulse Characteristics					Results from Particle-Pushing Code				Results from Simplified Model				$\dfrac{\dot{P}_{model}}{\dot{P}_{P.P.Code}}$	$\dfrac{\dot{E}_{model}}{\dot{E}_{P.P.Code}}$
End of Linear Portion of pulse (nsec)	Peak Emission Current (amp/m²)	Average Normal Electron Velocity (m/sec)	Maximum Emission Energy (keV)	Approx. Peak of Energy Spectrum (keV)	Peak $\dot{P}$ (amp/m)	Time of Peak $\dot{P}$ (nsec)	Peak $\dot{E}$ (V/m-sec)	Time of Peak $\dot{E}$ (nsec)	Peak $\dot{P}$ (amp/m)	Time of Peak $\dot{P}$ (nsec)	Peak $\dot{E}$ (V/m-sec)	Time of Peak $\dot{E}$ (nsec)		
10	10^5	3.54(+7)	70	1.0	134.6	1.12	1.52(+15)	1.34	134.5	1.13	1.73(+15)	1.53	1.0	1.14
10	10^4	3.54(+7)	70	1.0	62.5	2.42	3.28(+14)	2.90	62.5	2.42	3.72(+14)	3.29	1.0	1.13
10	10^3	3.54(+7)	70	1.0	29.0	5.2	7.10(+13)	6.28	29.0	5.22	8.0 (+13)	7.1	1.0	1.13
10	10^2	3.54(+7)	70	1.0	13.3	10.9	1.13(+13)	>t₁	13.3	11.0	1.13(+13)	15.3	1.0	1.0
6	1.67(+5)	2.59(+7)	25	1.0	117.6	0.70	2.84(+15)	0.90	112.4	0.72	3.08(+15)	1.0	0.955	1.08
6	2.24(+5)	2.59(+7)	25	1.0	122.4	0.65	3.17(+15)	0.75	123.9	0.65	3.75(+15)	0.89	1.01	1.18
10	2.24(+6)	2.98(+7)	50	1.0	282.7	0.36	1.06(+16)	0.42	284.5	0.38	1.3 (+16)	0.51	1.01	1.23
10	1.23(+6)	3.75(+7)	70	5.0	340	0.48	6.9 (+15)	0.50	341.7	0.50	9.4 (+15)	0.67	1.01	1.36
10	7.73(+5)	3.73(+7)	100	5.0	290	0.58	5.25(+15)	0.60	290.1	0.58	6.9 (+15)	0.78	1.0	1.31
10	5.14(+5)	4.12(+7)	120	5.0	302	0.73	3.92(+15)	0.68	298.9	0.69	5.4 (+15)	0.93	0.99	1.38
2	2.47(+4)	3.49(+7)	130	1.0	156.8	1.18	1.40(+15)	1.08	140.2	1.04	1.98(+15)	1.4	0.895	1.41
6	1.3 (+4)	3.48(+7)	130	1.0	85.7	1.98	4.5 (+14)	2.04	78.5	1.86	6.2 (+14)	2.5	0.915	1.38
6	1.3 (+2)	3.49(+7)	130	1.0	16.2	8.8	1.3 (+13)	9.3	15.4	8.2	1.47(+13)	11.7	0.95	1.13
2	7.95(+4)	2.39(+7)	45	1.5	123.3	0.72	2.78(+15)	0.74	110.7	0.62	3.8 (+15)	0.85	0.895	1.37
6	4.17(+4)	2.39(+7)	45	1.5	69.4	1.26	8.5 (+14)	1.58	61.9	1.11	1.2 (+15)	1.5	0.892	1.41
6	4.17(+2)	2.39(+7)	45	1.5	14.9	5.8	4.0 (+13)	6.0	13.3	5.17	4.7 (+13)	7.	0.892	1.17
17.5	410	1.72(+7)	14	1.5	5.56	7.8	1.9 (+13)	7.0	5.36	6.66	2.4 (+13)	0.9	0.965	1.26
17.5	51.2	2.08(+7)	14	3.5	4.0	16.0	4.8 (+12)	14.4	3.68	14.2	5.8 (+12)	19.3	0.92	1.21

problems in Table A-4, the emission particles were distributed linearly down to zero velocity. Thus, the spread in particle velocities about the average is greater. The result is that the simplified model gives consistently low values of the peak $\dot{P}$ relative to the values from the particle-pushing code, but they are still within about 10% of each other. Moreover, for comparing relative effects of different spectra and emission pulses, the simplified results would give almost the same results as the particle-pushing code.

The peak $\dot{E}$ values, as calculated by the simplified model, are consistently larger than the values from the particle-pushing code, as intended, except for the one case in which the peak $\dot{E}$ from the particle-pushing code occurred after t_1. In that case, the agreement is exact, as it should be. The largest discrepancy is about 41%, which is not too bad considering that the peak $\dot{E}$'s cover a range of over three orders of magnitude. Moreover, for relative comparison between spectra, the agreement is better because the errors in relation to the particle-pushing code are always in the same direction.

A subset of the results of Table A-4 is plotted in Figure A-4 for illustration purposes. (The highest current data points are for a slightly different energy spectrum than the others, and so the curve is dashed.) Excellent agreement between the two methods of calculation is shown over more than four orders of magnitude of emission current.

In summary, the simplified models provide a convenient method for estimating the peak values of $\dot{P}$ and $\dot{E}$ and their times of occurrence for a wide range of spectra and pulse shapes. The absolute values of the peak $\dot{P}$ and $\dot{E}$ from the simplified model are within about 10 and 40%, respectively, of the corresponding values from the one-dimensional particle-pushing code. Peak $\dot{E}$ values are consistently on the conservative (high) side, but peak $\dot{P}$ values are generally slightly low. For relative comparisons among different spectra and pulse shapes, the agreement of the simple model with the particle-pushing code is even better than the absolute agreement.

The above equations for the peak $\dot{P}$ and $\dot{E}$ and their times of occurrence are quite straightforward for programming on the TI-59 calculator, with the only required input quantities being the maximum emission current density (J_m), the time to this peak emission current (t_1), and the average velocity of the emitted electrons normal to the emitting plate. For convenience, this average normal velocity can be related to the average energy of the emitted electrons, assuming a particular angular distribution such as a cosine distribution.
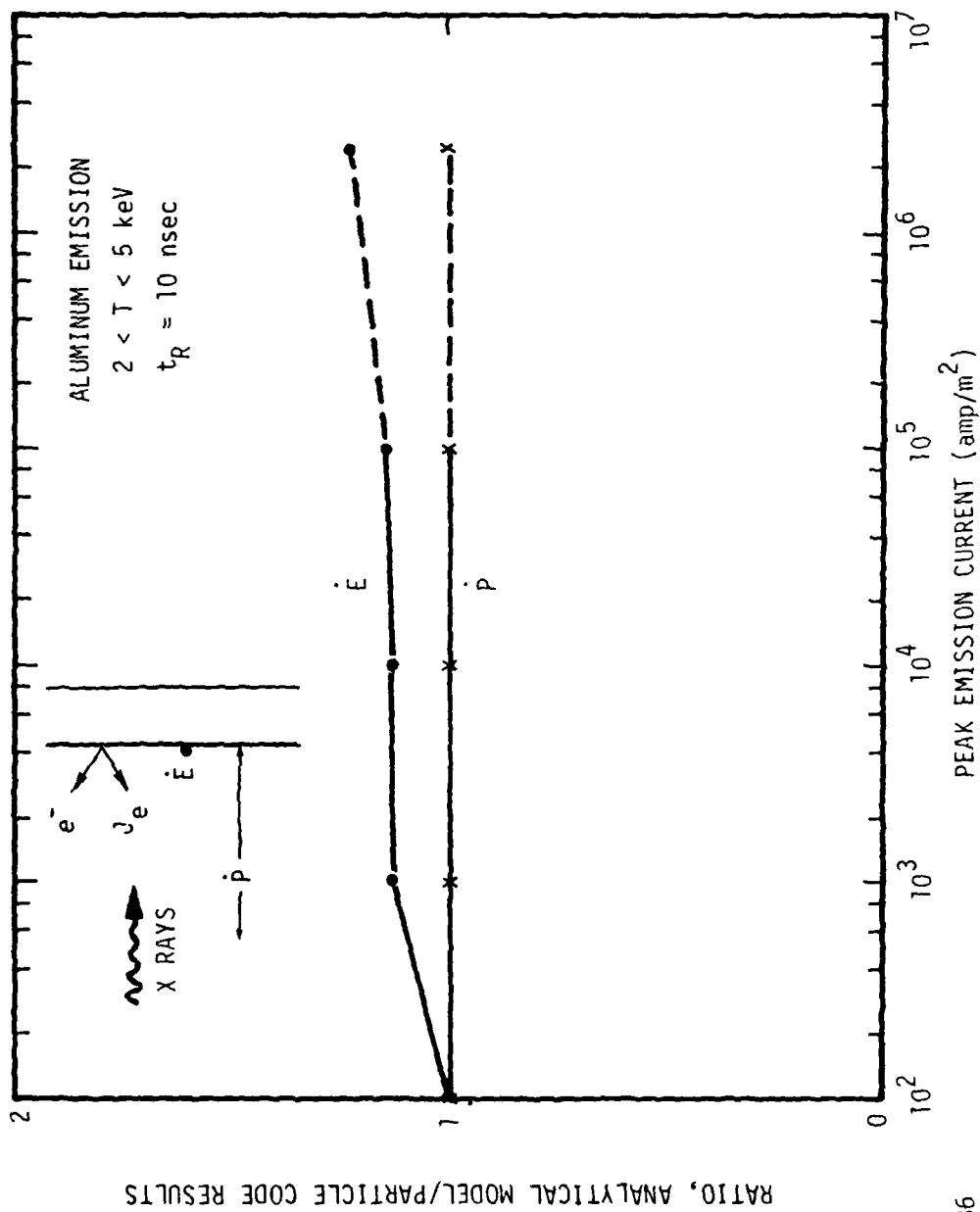
Figure A-4. Ratios of peak electric field and dipole moment rates of change above a plane for the present model compared to a particle-pushing code. The curves are based on the 10-nsec rise time results of Table A-4.

RE-02686

46

A.3.8   Estimate of Absolute Magnitude of Surface Skin Currents

Skin currents on the exterior surface of an illuminated conducting body scale approximately linearly with the rate of change of the space-charge dipole moment, $\dot{P}$, in the illuminated region (Ref. A-5). However, for application to quick assessments of radiation hardness, it would be more useful if the value of $\dot{P}$ could be used to estimate the absolute magnitude of the skin currents which it would produce on a body.

Other researchers (Refs. A-8, A-9) have addressed this problem by considering the skin currents induced on a conducting sphere of radius R by a single point charge q moving radially outward from the sphere with velocity v. When the point charge is close to the surface of the sphere, the skin current, I_θ (amp), on the sphere that crosses a cone with the half-angle θ about the velocity vector v (Figure A-5) is

$$I_\theta = \left(\cos\theta + \frac{\sqrt{2}}{\sqrt{1 - \cos\theta}} \right) \frac{vq}{2R} \; . \tag{A-19}$$

At the $\theta = 90°$ point, Eq. 2 reduces to

$$I_\theta = 0.707 \frac{vq}{R} \; . \tag{A-20}$$

In the more usual situation with an illuminated sphere, the emitted charge q would be spread over a finite area, probably a hemisphere, rather than being a single point charge. At a given point on the sphere -- e.g., the $\theta = 90°$ point, one would expect the skin current to be somewhat larger when the same amount of emitted charge is spread over a finite area because part of the emission area would be closer to the point where the skin current is monitored. To estimate the magnitude of this effect, a calculation has been made for the skin current crossing a cone with an angle θ when the charge q is emitted radially outward with velocity v with a uniform emission intensity σ over a spherical end cap that subtends a half-angle α_m at the center of the sphere (Figure A-6). The density σ is given by

$$\sigma = \frac{q}{2\pi R^2 (1 - \cos\alpha_m)} \; . \tag{A-21}$$

The skin current is obtained by calculating the time rate of change of the surface charge on the sphere inside the cone angle θ.
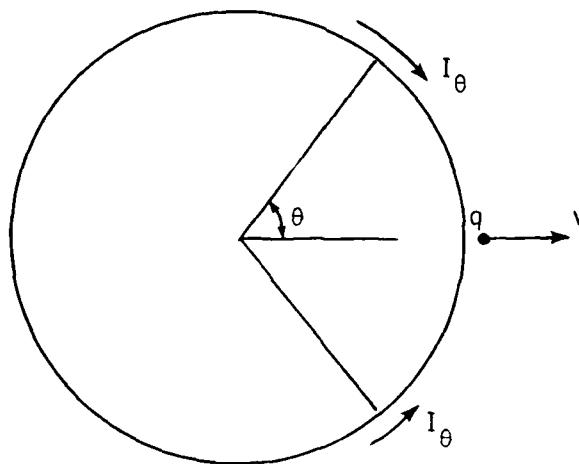
RE-03088A

Figure A-5. Geometry for point charge near a sphere
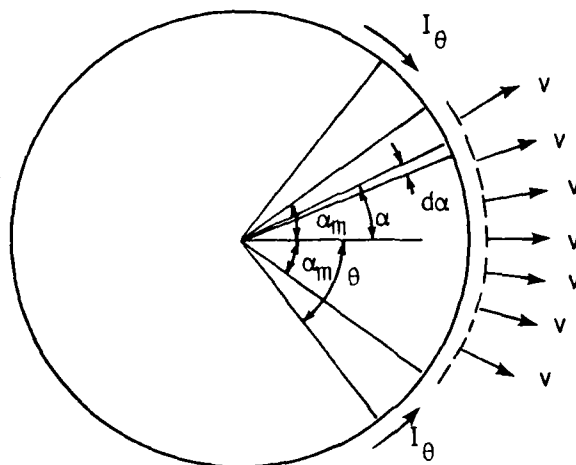
RE-03088B

Figure A-6. Geometry for distributed emission

If α and ϕ are the polar and azimuthal coordinates of a point on the sphere in the emitting area (Figure A-6) and the charge q is at a radius b slightly greater than R, the equation for the surface current is

$$I_\theta = \frac{v\sigma R^3}{2} \int_0^\theta \sin\theta' \, d\theta' \int_0^{2\pi} d\phi \int_0^{\alpha_m} \sin\alpha$$

$$\times \left(\frac{1}{b^2} + \frac{5b\ R^2 - b^3 - b^2\ RG - 3R^3\ G}{d^2} \right) d\alpha \ , \tag{A-22}$$

where

$$G = \sin\alpha \sin\theta' \cos\phi + \cos\alpha \cos\theta' \tag{A-23}$$

and

$$d^2 = R^2 + b^2 - 2b\ RG \ . \tag{A-24}$$

Equation A-22 has been integrated numerically for two different values of b slightly greater than R since the integrand becomes infinite for some angles when b exactly equals R. The integrated results for the two values of b were close enough together to give confidence that the results are not sensitive to this parameter in the integration.

The integration was also performed for two values of α_m (5 and 89°) corresponding approximately to a point charge and full hemispherical emission.

When the current at $\theta = 90°$ due to emission from the area defined by $\alpha_m = 5°$ is normalized to the emission area (Eq. A-21), the numerically integrated result is

$$I_{90°} = 0.67 \frac{vq}{R} \ , \tag{A-25}$$

which is close enough to Eq. A-20 to indicate that the numerical integration is reasonable.

When the numerically integrated value for $\alpha_m = 89°$ is normalized to its emission area, the result is

$$I_{90°} = 1.18 \frac{vq}{R} \ . \tag{A-26}$$

Thus, distributing the emitted charge q over a hemisphere increases the current at $\theta = 90°$ compared to the current due to a point charge by a factor of about 1.75.

For use with the $\dot{P}$ formulation, the quantity qv should be identified with $\dot{P}A$, where A is the emission area. For hemispherical emission ($A = 2\pi R^2$), the current density at $\theta = 90°$ is then

$$H_{\phi(90°)} = \frac{I_{90°}}{2\pi R} = 1.18 \ \dot{P} \ . \tag{A-27}$$

The symbol H_ϕ has been used to denote the azimuthal magnetic field which is numerically equal to the replacement current density at the conducting surface.

A.4 CABLE COUPLING

X-ray-induced cable signals can be imagined to result from four separate drivers:

1. Knock-on current (emitted electrons captured by the cable).

2. $\dot{B}A$ voltage source.

3. $\dot{C}V$ current source.

4. Photon-driven charge (differential charge transfer between the dielectric and the conductors of the cable).

These mechanisms are defined and discussed in the following sections. They are fairly well understood, so the objective of this study is to derive quick, simple means for estimating the relative and, if possible, the absolute magnitudes of cable responses due to different SGEMP pulses.

In this discussion, the word "cable" can mean the conductor of an unshielded cable, the conducting sheath of a shielded cable, or the outer conducting shield around a cable bundle. The currents that are estimated are the total currents on the cables or cable shields. It is beyond the scope of the present effort to atten pt to predict the penetration of current through the shield of a single cable or a cable bundle, or to estimate the division of the current between separate wires of a cable bundle.

In most situations, the radiation hardness analyst will not have a precise definition of the locations of the cables in his system, especially in the design stage before the final configuration is established. In that case, he is usually interested in worst-case values for scoping the magnitude of the problem and for pinpointing the potentially critical items that will need more refined estimates. Hence, the coupling formulas used herein assume worst-case locations and orientations of the cables. For example, for $\dot{B}A$ coupling, the cable is assumed to be oriented parallel to the conducting surface and perpendicular to the direction of the local magnetic field. Similarly, for $\dot{C}V$ coupling, the cable is assumed to be close to the emitting surface where the electric fields are largest.

A.4.1 Knock-On Current

Knock-on current is the <u>net</u> flux of electrons captured or emitted by the outside of a cable. This current must flow back to ground, mainly through the cable shield, but some fraction of it will couple into the center conductor of the cable, depending on how

50

effective the cable shielding is. The emission current from the cable is estimated by the simplified relations programmed into the TI-59 calculator, ignoring space-charge-limiting from the cable since cable sizes and distances to conducting structures are usually small compared to the width of the space-charge layer. Thus, in the present discussion, we will be concerned only with the amount of current captured by a cable due to emission from adjacent surfaces.

For very low fluxes, when space-charge-limiting is negligible, the capture current is just the emission current density from the surrounding surfaces times the appropriate projected area of the cable. However, when there is a significant space-charge potential barrier and the cable is not immediately adjacent to the emitting surface, the lower-energy emitted electrons cannot reach the cable because of the potential barrier. On the other hand, the higher-energy electrons will be able to reach the cable, and those electrons on a direct line with the cable will be immediately captured by it. Some of the nearby electrons that missed the cable on the outward flight will be turned back by the potential barrier and can then strike the cable on their way back to the emitting surface. Thus, a realistic estimate of the total capture current is crucially dependent on a knowledge of the potential-barrier profile in the region of the emitting surface (the space-charge region). This problem has been studied extensively in the SGEMP community, both for conducting cavities (short-circuited diodes) and for external surfaces (open-circuit diodes); see, for example, References A-10 - A-12. However, because of the complexity of the problem, most of the analytical studies have been restricted to steady-state conditions. Obviously, early in a pulse, before the potential barrier has been fully established, a larger percentage of the emitted current can reach a given cable position. Whether this initial surge of current is greater than the peak current in a fully developed barrier depends on the rate of rise of the emission pulse and the degree of space-charge limiting. Reference A-10 describes a complex computer code which treats the time-dependent problem, but results are not easily reduced to analytic solutions. Considerable simplification of the problem has been assumed for the calculator codes at present.

Knock-on current is the difference between (1) the current of electrons that is emitted from the illuminated surface of the satellite and is then captured by the cable and (2) the current emitted from the outer surface of the cable by the incident photons. For worst-case estimates, it is conservative to consider the captured and emitted currents separately, since they always produce cable currents of opposite signs.

51

For the emitted current, the current per unit length of cable can be taken as the circumference of the cable times the larger of the reverse or forward yield from the cable, divided by the photon pulse width (FWHM). These yields can be obtained by the routines described in Section A.2. In all these calculations of knock-on current, the relevant cable radius corresponds to its outermost surface, whether the latter is a conductor or a dielectric.

For the captured current, the magnitude depends on the height of the potential barrier relative to the energy spectrum of emitted electrons and the location of the cable relative to the position of the peak in the potential. However, for worst-case estimates, it can be assumed that the cable is fairly close to the emitting surface and that the potential barrier is large enough that practically all the emitted electrons are reflected back to the emitting surface. Thus, the cable will capture electrons on both its front and back sides. Except for a slight time delay for the emitted electrons to be reflected from the potential barrier, the instantaneous knock-on current due to the captured electrons is just

$$I(t) = 4a \ell J_{em}(t) , \qquad (A-28)$$

where $4a \ell$ is twice the projected area of the cable and $J_{em}(t)$ is the instantaneous emission current density.

A.4.2 $\dot{B}$ Coupling

This coupling mechanism is the voltage induced in a conducting loop by the rate of change of the magnetic flux lines enclosed by that loop.

As mentioned previously, the B fields on the outside of a photo-illuminated body are proportional to $\dot{P}$, the rate of change of the space-charge dipole moment. Thus, a relative comparison of $\dot{B}$ coupling can be obtained by comparing the peak $\ddot{P}$'s for different excitations. However, for system coupling studies, one needs absolute values of the magnetic fields, and very often one needs them inside conducting cavities.

Consider a cable with the centerline above a conducting surface, h, and the length ℓ defining the coupling area $(A = h\ell)$. If the cable is close to a surface, the driving B field is the one due to the returning skin current, K_s (amp/m), which is caused by the rate of change of the space-charge dipole moment $\dot{P}$. In that case, the driving voltage in the circuit is

$$\dot{B}A = \mu_0 A \frac{dK_s}{dt} = \mu_0 A K_{\dot{P}} \ddot{P} , \qquad (A-29)$$

52

where μ_0 is the magnetic permeability of free space, $K_{\dot{P}}$ is the constant proportionality between $\dot{P}$ and the skin current K_s at the point of interest on the body, and $\ddot{P}$ would be obtained as described in Section A.3.4.

For $\dot{B}A$ coupling inside a conducting cavity, the return currents on the walls of the cavity will be a function of the rate of change of the space-charge dipole moment $\dot{P}$ in the cavity and the portion of the emitted current that surmounts the space-charge potential barrier and is transmitted across the cavity. For large cavities, high fluences, and/or very short pulses, the contribution of $\dot{P}$ to the peak surface currents should exceed the contribution from the transmitted current. On the other hand, for small cavities, low fluences, and/or long pulses, the surface currents will be determined primarily by the transmitted current.

For $\dot{B}A$ coupling due to the transmitted current in a conducting cavity, it is conservative for present purposes to assume that the depth of the cavity is small so that space-charge-limiting will be minimal. It is assumed that the user will input a characteristic dimension (2R) of the cavity normal to the incident beam. Assuming that this cavity is a cylindrical can of radius R which is illuminated from one end, the maximum magnetic field, H, will be adjacent to the cylindrical wall and will have a magnitude

$$H = J_{em} \frac{R}{2} , \tag{A-30}$$

where J_{em} is the internal emission current density (amp/m^2) from the end of the cylinder. The assumption of a cylindrical cavity gives an upper-limit estimate of the return current densities, except for local effects, because a cylinder has the smallest possible ratio of circumference to cross-sectional (emission) area. The resulting $\dot{B}A$ voltage is

$$\dot{B}A = \mu_0 A\dot{H} = \mu_0 A \frac{R}{2} \frac{dJ_{em}}{dt} . \tag{A-31}$$

The amount of current that will flow on the cable as a result of the $\dot{B}A$ voltage will depend on its inductance, L, and its termination resistance, Z_R. For a simple circuit with L and Z_R in series (Figure A-7) and driven by a step voltage $\dot{B}A$, the resulting current in the cable is

$$I(t) = \frac{\dot{B}A}{Z_R} [1 - \exp(-tZ_R/L)] . \tag{A-32}$$

53
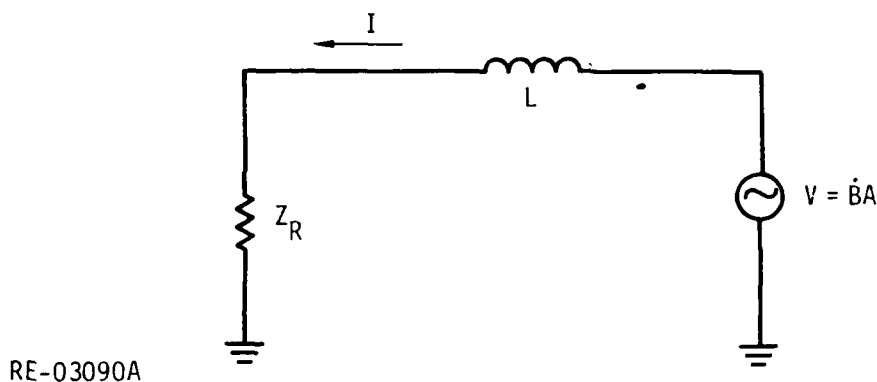
RE-03090A

Figure A-7. Simplified equivalent circuit for $\dot{B}A$
driver excitation of a cable

For a large value of Z_R, the exponential term damps out before the driving voltage ($\dot{B}A$) decays away. In that case, the peak I is just $\dot{B}A/Z_R$. However, for essentially short-circuit conditions ($Z_R \simeq 0$), the current I will increase linearly with time for the duration of the voltage driver (t_p), so the peak current is

$$ I_p = \frac{\dot{B}A\ t_p}{L} = B_{max}\ A/L \tag{A-33} $$

for a constant $\dot{B}$.

It is assumed that the user will input his termination impedance, Z_R, or use a default value of 50 ohms. In addition, if the short-circuit condition applies, he must input the radius of his cable or cable bundle, a, in addition to the previously inputted height of the cable centerline above the conducting plane, h. The code will then calculate the inductance L from the following formula for a cylindrical conductor over a ground plane.

$$ L = \frac{\mu_0\ \ell}{2\pi}\ \ell n\ \left(\frac{h + \sqrt{h^2 - a^2}}{a}\right). \tag{A-34} $$

A.4.3 $C\dot{V}$ Coupling

When the voltage V between two conductors changes with time, the resulting driver for an equivalent electrical circuit can be represented by a current source $C\dot{V}$, where C is the capacitance between the conductors. As mentioned previously, for worst-case estimates it is assumed that the cable is close to the emitting surface where the electric fields are largest, either on the exterior of a satellite or in an interior cavity. For the present purposes, it is conservative to ignore the decrease in the electric field with

54

distance from the emitting surface, due either to the space-charge cloud or to the image charges in the opposite wall of a cavity.

Using the peak value of the rate of change of the surface electric field, $\dot{E}$, the peak $\dot{V}$ is just $\dot{E}h$, where h is the height of the cable above the emitting surface. Using the radius of the cable a and the cable length ℓ, the capacitance C for a cylinder over a ground plane can be written as

$$C = \frac{2\pi\ell\varepsilon_0}{\ln\left(\frac{h + \sqrt{h^2 - a^2}}{a}\right)} \quad , \qquad (A-35)$$

where ε_0 is the permittivity of free space. Note that Eqs. A-34 and A-35 yield a propagation velocity along the cable equal to the speed of light, as they should.

For the simple circuit shown in Figure A-8, the current I in the cable due to a step current driver $h\dot{E}C$ is

$$I(t) = A_1 \exp(-s_1 t) + A_2 \exp(-s_2 t) + h\dot{E}C \quad , \qquad (A-36)$$

where

$$s_{1,2} = 0.5 \frac{Z_R}{L} \pm \sqrt{(Z_R/L)^2 - 4c/L} \quad , \qquad (A-37)$$

and A_1 and A_2 are constants determined by the boundary conditions.

RE-03090B
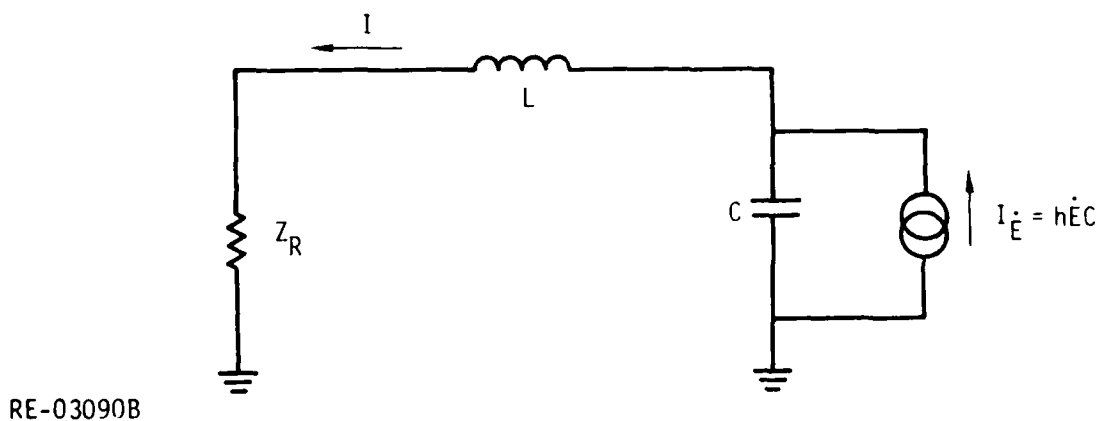
Figure A-8. Simplified equivalent circuit for $C\dot{V}$ excitation of a cable

If the duration of $\dot{E}$ is long compared to the damping times $1/s_1$ and $1/s_2$, the peak current in the cable will be the steady-state value $h\dot{E}C$. However, if R is very large, Eq. A-36 is approximately

$$I(t) \simeq h\dot{E}C\{1 - \exp[-t(/Z_R\,C)]\} , \qquad\qquad (A-38)$$

so $I(t)$ initially increases linearly as

$$I(t) \simeq h\dot{E}t/Z_R , \qquad\qquad (A-39)$$

and the peak current is

$$I_p = hE_{max}/Z_R . \qquad\qquad (A-40)$$

To scope the cable current when the termination impedance is uncertain, the peak current should be calculated both by Eq. A-40 and from the steady-state value $h\dot{E}C$, and the larger value should then be used.

A.4.4 Photon-Driven Current

When photons are incident on a cable or a cable bundle, electrons are emitted from the cable conductors and are trapped in the cable dielectrics. This displacement of charge causes a potential difference between the cable core and shield, which drives a current between the two conductors. This current is called the photon-driven current.

Extensive work is reported in the literature on measurements and predictions of these currents (see, for example, Refs. A-13 - A-15). The magnitude of the current, or the total charge transfer during the pulse, is a function of the cable geometry and materials and of the energy spectrum and intensity of the emitted electrons. An estimate of the relative magnitudes of this current in a given cable in vacuum due to different photon pulses can be made by comparing the dipole moment, D, of the charge emitted from the cable conductors and captured in the dielectrics. This dipole moment is just the product of the emission yield times the average range of the emitted electrons in the dielectric, including gaps between the cable conductors and the dielectrics. The absolute magnitude of this cable response can be estimated by integrating the effect of D around the circumference of the cable, near both the center and outer conductors. This integration has been done fairly successfully for coaxial cables graphically (Ref. A-7) and with a computer code (Ref. A-15). However, both these approaches require considerable reduction to fit into present programmable calculators such as the TI-59.

The present expression employed on the calculator is

$$I = 2\Phi P\ell/\Delta T \ ,$$

where Φ is the fluence (cal/m^2), P is the dipole moment per unit area of the electrons emitted by the shield into the dielectric material (C-m/cal), ℓ is the cable length (m), and ΔT is the x-ray pulse width (sec). P is based on the simple planar geometry value in the data base obtained with the QUICKE2 electron code. P can be replaced by the electron yield times a gap width if one exists, and if that product is greater than P. The approximation provides better than order-of-magnitude estimates, and should scale properly with x-ray and material parameters when compared with more exact calculations.

A.4.5 Summary of Cable Drivers

The cable coupling terms are summarized in Figure A-9. The upper right corner defines spectrum and geometry parameters where $\dot{\Phi}$ is the x-ray flux (cal/m^2/sec), $\mathcal{E}$ indicates the energy spectrum, τ is the attenuation material mass (g/cm^2), Z is the atomic weight of the electron emission material, I_e is the emitted electron current (amp/m^2), and the other input variables are self-explanatory. L and C are the cable inductance and capacitance per unit length, respectively. $\dot{E}$ and $\dot{B}$ are the electric and magnetic field rates.
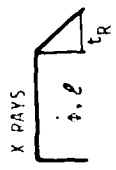
GROUND PLANE

R = 0 TERMINATION

CABLE

X RAYS

τ, z

h

ℓ

t_R

LET $g = \ell n \, [h/a + \sqrt{(h/a)^2 - 1}]$

KNOCK-ON CURRENT:

$I = J_e \cdot A_e$

$J_e (\ell, \tau, \ldots, \Phi, z)$ FROM CALCULATOR

BA VOLTAGE:

$I = \ldots$, P $(\ell, \ldots, \Phi, z)$ FROM CALCULATOR , $L = \frac{\mu_0}{2\pi} \ell g$

CV CURRENT:

$I = \ldots$, E (ℓ, τ, Φ, z) FROM CALCULATOR

DIRECT-DRIVE CURRENT:

$I \approx \frac{2 P \varepsilon \phi}{\Delta t}$, P (ℓ, τ, z) FROM CALCULATOR

SHIELD

CENTER CONDUCTOR

DIELECTRIC

RE-03188
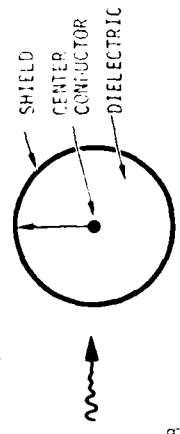
Figure A-9. Summary of cable current expressions for low-impedance terminations

58

REFERENCES

A-1.   F. Biggs and R. Lighthill, "Analytical Approximations of X-Ray Cross Sections, II," SC-RR-71 0507, December 1971.

A-2.   S. Rogers and A. Woods, "Multiple Plate Modification of the QUICKE2 Electron Emission Code," DNA 4062T, June 1976.

A-3.   A. J. Woods and E. P. Wenaas, "Photon Source SGEMP Spectrum Evaluations," DNA 5261F, April 1978.

A-4.   T. A. Dellin and R. E. Huddleston, "Second-Generation Analytical Photo-Compton Current Methods," IEEE Trans. Nucl. Sci. NS-22, No. 6, December 1975.

A-5.   A. Wilson and D. Parks, IEEE Trans. Nucl. Sci. NS-23, No. 6, December 1976.

A-6.   E. Waisman et al., IEEE Trans. Nucl. Sci. NS-25, No. 6 (1978), p. 1336.

A-7.   N. J. Carron and C. L. Longmire, "On the Structure of the Steady-State Space-Charge-Limited Boundary Layer in One Dimension," DNA 3928T, November 1975.

A-8.   E. P. Wenaas, "Structural Coupling Estimates for Spacecraft Charging and Discharging," JAYCOR report EED-76-003, prepared for Computer Sciences Corp. and Air Force Weapons Laboratory, July 1976.

A-9.   E. P. dePlomb, IEEE Trans. Nucl. Sci. NS-23, No. 6, December 1976, p. 1909.

A-10. A. J. Woods and T. N. Delmer, "The Rod-Over-Ground-Plane Code TEDIEM-PC," AFWL-TR-74-313, November 1974.

A-11. P. D. Gianino and T. M. Costello, "Space-Charge Limitation of Radiation-Induced Secondary-Electron Emission Currents in Evacuated Diodes," J. Appl. Phys. 47, No. 3, March 1976.

A-12. F. Hai, "Summary of Cable Response Experiments," Aerospace Corp., January 1976.

A-13. D. Clement and C. Wuller, "Assessment of Cable Response Sensitivity to Cable and Source Parameters in Low-Fluence X-Ray Environments," DNA 4407T, April 1977.

A-14. R. Leadon et al., "Radiation Effects in Satellite Cables," HDL-CR-78-089-1, April 1978.

A-15. D. Tasca et al., IEEE Trans. Nucl. Sci. NS-25, No. 6 (1978), p. 1382.

APPENDIX B

USER'S INSTRUCTIONS FOR
PROGRAMMABLE CALCULATOR CODES FOR SGEMP EFFECTS

B.1   FOREWORD

This appendix provides step-by-step instructions to the SGEMP analyst for operating the calculator codes described in the main body of this report. The programs are designed for use on the Texas Instruments TI-59 calculator and do not require a printer or any other special options. Codes and data are read in from magnetic cards, and the user keys in selected parameters describing the x-ray environment and satellite structure.

The steps required by the user are to (1) specify the x-ray spectrum, (2) attenuate it to the satellite location of interest, (3) compute SGEMP excitation parameters, (4) compute SGEMP response parameters, and finally (5) compute cable current drivers. Each of these analysis functions is addressed by a separate small program in the calculator which is read in at the beginning of each step. Abbreviated job descriptions and their related calculator codes are listed in Table B-1. The codes are listed in the logical flow of analysis from specification of the x-ray environment to calculation of cable current drivers. The codes generally flow together in that, where possible, data from one program used by another does not have to be manually handled between steps. The second program simply picks it up from where it is located and proceeds.

The user is assumed to have elementary knowledge of the calculator's operation. Some general calculator and code characteristics are discussed in Section B.2. The individual programs are described in detail in Sections B.3 through B.7. A complete sample problem is described in Section B.8.

Table B-1. Calculator Codes for SGEMP Analysis Steps
(Parentheses around a program name indicate that it is optional)

Code Name	Function
None Required	Specify x-ray spectrum
(TBLSET)	Specify arbitrary x-ray spectrum
(BLKBDY)	Specify blackbody x-ray spectrum
ATTEN	Attenuate x rays
EXCITE	Calculate electron yield, velocity, and dipole moment in dielectrics
RESPONSE	Calculate E&M response parameters
CABLE	Calculate cable current drivers

61

B.2   USER INSTRUCTIONS COMMON TO ALL PROGRAMS

This section describes procedures common to all of the programs in this appendix.

A brief overview of the codes is helpful in understanding their operation. The calculator memory is divided into four banks which can be programmed with up to 240 steps each. Memory can be partitioned to interchange code steps and data storage, with up to 30 numbers stored in each bank. One insertion of a magnetic card sets all locations in a bank of memory. As an example, in the program EXCITE, the memory has been programmed according to the divisions shown in Table B-2. The memory allocation shown limits the program to only 240 steps, but it has the considerable advantage of permitting spectra to be stored on one set of cards and excitation parameter data on another set. The user may read in a spectrum to bank 2 and computer parameters for different satellite configurations by simply reading in different data to bank 3 and repeating the calculation.

Table B-2. TI-59 Memory Allocation for Computation of
Spectrum Evaluation Parameters, Program EXCITE

Bank 1	Program	Up to 240 steps
Bank 2	Spectrum	Up to 14 point pairs
Bank 3	Excitation parameter curves	Up to 15 point pairs
Bank 4	Working storage	

Magnetic cards are labeled according to information on the top or bottom half of the magnetic strip on the back. The arrows in the corners indicate the direction in which the card is to be fed into the right-hand slot on the calculator. The card is rotated to read in the right-hand arrows, not turned over (the user can always see the labeling). The upper label on the card pertains to the left-hand arrow, the lower to the right.

The calculator memory is partitioned differently in different sections of the system. Program and data cards are marked in the lower right-hand corner in terms of the number of program steps and data storage locations existing in the memory at the time the card was written. The default setting of the calculator is 479.59, indicating 480 program steps and 60 data storage locations, corresponding to a 50-50 division of the memory (data storage location requires eight program-steps' worth of memory). Cards written at default partitioning are not marked. The repartitioning of the memory is accomplished by pressing n Op 17, where n is the number of decades of data storage desired. For example,

62

many of the programs and data use the partitioning of 239.89, or 240 program steps and 90 data locations. This is accomplished in memory by pressing 9 Op 17. To examine the partitioning at any time, press Op 16.

The calculator labels are the keys in the top row (A-E, A´-E´). These are special-function keys which can be used to perform tasks automatically. For example, data can be stored in the correct location automatically by the program when the user enters his number and presses special-function key A, instead of having to specify the exact location in memory (using a STO 30 operation, for example).

B.3   X-RAY SPECTRUM INPUT

The x-ray spectrum is stored in the calculator in locations 60-73 (energy in keV) and locations 75-88 (differential fluence in units of $cal/cm^2/keV$). These values can be entered manually, or with optional routines described below, or they may be already in existence on a magnetic card. To perform manual entry, values for energies and fluences are stored by hand, with the user keeping track of the storage location. To input a spectrum without having to simultaneously keep track of the location within the calculator, refer to the instructions for the program TBLSET later in this section. To specify a black-body spectrum automatically, see the instructions for program BLKBDY. To read in a spectrum already on a data card, partition the calculator to the same partitioning it had when the card was written, press CLR, and insert the card. The calculator will display '2,' indicating that memory bank 2 has been loaded.

Spectra must have at least three energy bins, and must have a zero following the last entry (the zero should be in location 74 for spectra having the maximum of 14 energy bins). The present data base for photoemission excitation parameters is limited to the range 1 to 1000 keV, so x rays should be defined in this range only. Normalization to unit incident fluence is accomplished automatically by the EXCITE program.

To save a spectrum on a card, press CLR, 2, WRITE, and insert a card to be written. The card may be subsequently read to specify a spectrum by simply pressing CLR and inserting the card, as described above. It is suggested that the calculator partitioning at the time of writing the card be placed on the card to prompt the user attempting to read in that spectrum.

The recipes for different spectrum input methods are given in the following.

B.3.1 Manual Spectrum Input

Enter a value for energy into the calculator and press STO n, where n is the appropriate storage location, 60 < n < 73. Enter a value for differential fluence and press STO m, where m is the appropriate location, 75 < m < 88. Bin 1 energy is in location 60, differential fluence in 75, bin 2 energy in 61, etc. Observe general rules for spectra mentioned in the beginning of Section B.3.

B.3.2 Optional Spectrum Input Program: TBLSET

A routine is available to expedite table entries and checkouts. The routine is designed for generalized table entry at arbitrary locations in memory. In the present case, a string of energies must be placed into memory beginning at location 60, and the corresponding differential fluences beginning at location 75.

To perform this operation, press 9 Op 17 to partition memory, then CLR, then read in the TBLSET code card. Press RST, then R/S. The calculator now displays 1., indicating that the calculator is ready to receive the energy value for energy bin 1. Energies may now be input by keying them in and pressing R/S. The index of the next bin then appears. To indicate the last bin, enter a zero and the calculator will automatically skip to location 75 and display 1., indicating that the calculator is ready to receive differential fluence for bin 1. At this point, begin entering differential fluences and pressing R/S. Stop after the last bin.

The values may be displayed in succession by pressing E and then R/S, R/S, etc. Displays beginning at any location can be commenced by entering the desired location and pressing A'. The calculator will automatically begin displaying at location 60 if no entry is made into A'.

A summary of TBLSET operations is given in Table B-3.

Table B-3. Summary of Input/Output Routing TBLSET Instructions

Labels:	A'	B'	C'	D'	E'
	Starting location for display (default = value in B)		Starting location to multiply, R/S, multiply by R/S		
		B	C	D	E
		Starting location for storage (default = 60)			Display values beginning at A'

Table B-3. Summary of Input/Output Routing TBLSET Instructions (Cont.)

Press 9 Op 17.

Press CLR.

Read in program TBLSET.

Press RST, R/S.

Enter beginning storage location in B (default value = 60).

Enter energy, press R/S, energy, R/S, etc.

Terminate string with 0., R/S.

Enter differential fluence, press R/S, etc.

To display values, press E, R/S, R/S, . . .

To display values beginning at a location other than B, enter the location in A´

after RST, then press E, R/S, R/S, . . .

To save the spectrum on a card, press CLR, 2, WRITE, and insert a magnetic

card.

B.3.3   Optional Blackbody Spectrum Generator Program: BLKBDY

Setup

Partition the calculator to 240 program steps and 90 data locations.

Press 9 Op 17. 239.89 will be displayed.

Press CLR.

Insert program card (BLKBDY0. 1. will be displayed.

Input

A. Number of bins -- i.e., the number of (energy, differential fluence) pairs desired;

a minimum of three bins and a maximum of 14 bins can be specified.

-    Enter the number of bins desired into the calculator and press A.

B. Blackbody temperature (keV).

-    Enter the blackbody temperature into the calculator and press B.

C. Normalization fluence, Φ (optional).

Units as user's choice.

The blackbody spectrum is normalized so that the total fluence equals Φ. (The

default is $\Phi = 1$.)

-    Enter the total fluence Φ into the calculator and press C.

Execution

-    Press E to execute.

	Location
Energies (keV)	60-73
Differential fluences (cal/cm^2/keV)	75-88

- To save the spectrum on a magnetic card, press CLR, 2, WRITE, and insert a card.

Cautions

A. For blackbody temperatures T greater than 80 keV, the spectrum obtained with BLKBDY could give erroneous results when used in EXCITE. This problem arises because the blackbody spectrum for $T > 80$ will contain energies greater than 1000 keV and the excitation parameter data base used in EXCITE is valid only for energies from 1 to 1000 keV.

B. If BLKBDY is executed twice in a row and the number of bins is changed, the blackbody temperature and normalization constant must also be re-entered.

B.4   ATTENUATION PROGRAM: ATEN

Setup

Partition calculator to 240 program steps and 90 data locations.

- Press 9 Op 17.   239.89 will be displayed
- Press CLR.
- Insert program card (ATEN).   1. will be displayed

Input

A. Energy spectrum input -- see Section B.3.

B. Attenuation material data.

1. X-ray cross-section data: Data necessary for calculation of the cross section is stored in locations 21-29. Cards are available for low-Z ($Z \leqslant 29$) and high-Z ($Z > 29$) materials, where Z is the atomic number. To read in the card, press CLR and insert the card appropriate to the material of interest (either high- or low-Z). The calculator will display 4., indicating that the data has been stored in memory bank 4.

2. Mass per unit area, τ (g/cm^2), of the attenuation material: To read in τ, enter the value for τ into the calculator and press A.

3. Attenuation material atomic number, Z: To read in Z, enter its value into the calculator and press C.

66

Execution

The calculator is ready to calculate the total incident fluence, the attenuated spectrum, and the total attenuated fluence.

A. Total incident fluence, ϕ_T^{in} (cal/cm^2) (optional). If ϕ_T^{in} is desired, press $\underline{E'}$. At the termination of the calculation, ϕ_T^{in} is displayed. This optional step integrates the incident spectrum without modifying it.

B. Attenuated spectrum. Press $\underline{E}$. When the display is fixed, the attenuated spectrum has been stored in the appropriate data registers. This step alone simply stores the values and does not print out the integrated fluence.

C. Total attenuated fluence, ϕ_T^{attn} (cal/cm^2) (optional). If ϕ_T^{attn} is desired, press $\underline{E'}$ after B above is accomplished. At the termination of the calculation, ϕ_T^{attn} is displayed. This step is done after B above if it is done at all.

As an example, if the user has entered his spectrum and wants to know the incident and attenuated fluences, he presses $\underline{E'}$, $\underline{E}$, and then $\underline{E'}$ again. If he only wants the attenuated fluence, he presses $\underline{E}$ and then $\underline{E'}$. If he intends to execute EXCITE for his next step, the integrated fluence is computed automatically and step $\underline{E'}$ is not necessary in ATEN.

Attenuation Through Several Materials

A given incident spectrum can be attenuated through any number of materials. For example, for two materials, material 1 and material 2: First input the incident energy spectrum and attenuation material data for material 1. Execute the program. The attenuated spectrum from material 1 is now the incident spectrum of material 2 and is already stored in the proper data locations. Therefore, enter the appropriate attenuation material data for material 2. When the program is executed, the resulting spectrum has been attenuated through both material 1 and material 2. This can be repeated for any number of materials.

B.5   EXCITATION PARAMETER PROGRAM: EXCITE

Setup

Partition calculator memory to 240 maximum program steps with 90 data locations:

-   Press $\underline{9\ Op\ 17}$

-   Press $\underline{CLR}$.

-   Insert program card (called EXCITE).

Calculator will display 1., indicating that bank 1 has been programmed.

67

Excitation Parameter Data Input

Read selected excitation parameter data into locations 30-59 (bank 3):

- Press CLR.
- Insert card.

Calculator displays 3., indicating that bank 3 has been programmed.

Execution

The calculator is now ready to compute the selected parameter for the spectrum chosen.

- Press RST.
- Press R/S.

Execution commences and numbers flash on the display for each energy bin in the order below.

ε_i i^{th} bin energy (keV)

$\Phi_{0\varepsilon_i}$ i^{th} differential fluence (cal/cm^2/keV)

$\sum_i \Phi_{0\varepsilon_i} \Delta\varepsilon_i$ cumulative sum of fluences in each bin (cal/cm^2)

When the display becomes fixed, the value is total fluence:

$$\sum_{i=1}^{Nbins} \Phi_{0\varepsilon_i} \Delta\varepsilon_i \qquad (cal/cm^2) \,,$$

where Nbins is the total number of energy bins. This is the total fluence incident at the emission surface of the excitation parameter configuration.

- Press R/S.

Calculator displays excitation parameter P (per unit fluence on the emitting material). P represents any excitation parameter.[*]

- Press R/S.

---

[*] Warning: EXCITE gives the photoelectron yield, for example, per unit fluence at the emission location. The x-ray shinethrough fraction must then be multiplied in to obtain the total yield for x-ray fluence on the outside of the attenuating material.

Calculator displays ratio $P_{previous}/P_{current}$, the ratio of the previously calculated excitation parameter to the current one. Thus, if the velocity is being computed, for example, the yield (for velocity calculation) is computed first, then a new card read in for yield/velocity and the process repeated. The third static display yields the ratio yield/(yield/velocity) = velocity.

B.6   RESPONSE PARAMETER PROGRAM: RESPONSE

Setup

Response is stored on two magnetic cards and occupies banks 1-3 in the calculator. Banks 1 and 2 are stored on one card and bank 3 on the second card. The calculator must be partitioned to 560 program steps and 50 data locations.

- Press 5 Op 17.   559.49 will be displayed.
- Press CLR.
- Insert program card RESPONSE, bank 1.   1. will be displayed.
- Press CLR.
- Insert program card RESPONSE, bank 2.   2. will be displayed.
- Press CLR.
- Insert program card RESPONSE, bank 3.   3. will be displayed.

Input

The input parameters must be manually stored into the following storage locations.

Parameter		Storage Location
t_R	Pulse rise time (sec)	10
Δt	FWHM, pulse full width at half maximum (sec)	12
Φ	Total fluence (cal/m^2)	13
Y	Yield (C/cal)	16
v_{ave}	Average normal velocity (m/sec)	17

For example, if t_R = 10 nsec,

- Press 1 EE +/- 8.
- Press STO 10.

Proceed similarly for Δt, Φ, Y, and v_{ave}.

Execution

To execute RESPONSE:

- Press RST.
- Press R/S.

69

The calculator display will become fixed when all parameters have been calculated. RESPONSE calculates values for the output parameters and stores the values in the following locations.

Parameter		Storage Location
J_{em}	Peak emission current (amp/m^2)	15
$\dot{P}$	Peak time rate of change of the space-charge dipole moment (amp/m)	20
$\ddot{P}$	Peak time rate of change of $\dot{P}$ (amp/m-sec)	21
$\dot{E}$	Peak time rate of change of electric field (V/m-sec)	22
E	Peak electric field (V/m)*	23
t_{m1} t_{m2}	Time of peak $\dot{P}$ (whichever is non-zero)	18 19
t_{m3}	Time of peak $\dot{E}$, time for $\dot{P} = 0$ (sec)	26

*If the value for E is zero, the problem was computed to be non-space-charge-limited, for which no formula for E has provided in the programs. The value for E is simply $J_E \Delta t / \varepsilon$, however, in that case.

For example, the value for $\ddot{P}$ can be displayed in the calculator by pressing <u>RCL 21.</u>

RESPONSE can be executed for other input parameters by simply changing the ones being varied and pressing <u>RST,</u> <u>R/S.</u> It is not necessary to reenter parameters held constant.

B.7   CABLE CURRENT PROGRAM: CABLE

<u>Setup</u>

The program CABLE is stored on two sides of one magnetic card and occupies banks 1 and 2 in the calculator. The calculator must be partitioned to 560 program steps and 50 data locations.

-    Press <u>5 Op 17.</u>   559.49 will be displayed.
-    Press CLR.
-    Insert program card CABLE, bank 1   1. will be displayed.
-    Press CLR.
-    Insert program card CABLE, bank 2   2. will be displayed.

70

Input

A. Response quantities. The necessary response quantities can be entered by running the program RESPONSE or they can be manually stored into the calculator memory.

1. Inputs from RESPONSE: CABLE has been designed to use as input results obtained by executing the program RESPONSE. All necessary response parameters are calculated by RESPONSE and stored in the correct locations for use in CABLE.

2. The necessary response quantities can also be manually entered into the calculator. These response parameters must be stored in the following locations. None of these parameters needs to be specified if RESPONSE has been executed previously.

Parameter		Location
ϵ_0	Permittivity of free space = 8.854×10^{-12}	00
t_R	Pulse rise time (sec)	10
Δt	FWHM, pulse full width at half maximum (sec)	12
J_{em}	Peak emission current (amp/m^2)	15
$\dot{P}$	Peak time rate of change of the space-charge dipole moment (amp/m)	20
$\ddot{P}$	Peak time rate of change of $\dot{P}$ (amp/m-sec)	21
$\dot{E}$	Peak time rate of change of electric field (V/m-sec)	22
E	Peak electric field (V/m)	23

Inputs

The cable inputs are the cable standoff, cable length, cable radius, termination impedance, and cavity diameter. Not all of these parameters are necessary inputs in calculating the various currents. Consult Section B.7 to determine which inputs are required for the current(s) of interest.

The cable inputs are entered as follows.

- Cable standoff, h (m)

   Enter value for h.

   Press A′.

- Cable length, ℓ (m)

     Enter value for ℓ.

     Press C´.

- Termination impedance, Z_R (ohm)

     Enter value for Z_R (value must be zero).

     Press D´.

- Cable radius, a (m)

     Enter value for a.

     Press E´.

- Cavity diameter, 2R (m)

     Enter value for 2R.

     Press E.

Execution

Listed below are execution instructions for the various currents and inputs needed for each current (see paragraph B under "Input").

A. Surface skin current density (numerically equal to tangential magnetic field H_ϕ) , H_ϕ (amp/m)

     Press A. The value for H_ϕ is displayed and also is stored in location 26.

B. $\overset{\bullet}{B}A$ currents, $I_{\overset{\bullet}{H}}$ (amp)

- Exterior $\overset{\bullet}{B}A$ current, $I_{\overset{\bullet}{H}}^{ext}$

     Cable inputs needed -- h, ℓ, Z_R, a

          Press B. The value for $I_{\overset{\bullet}{H}}^{ext}$ is displayed and stored in location 27.

- Interior $\overset{\bullet}{B}A$ current, $I_{\overset{\bullet}{H}}^{int}$

     Cable inputs needed -- h, ℓ, 2R, Z_R, a

          Press B´. The value for $I_{\overset{\bullet}{H}}^{int}$ is displayed and stored in location 28.

C. $\overset{\bullet}{C}V$ current, $I_{\overset{\bullet}{E}}$ (amp)

     Cable inputs needed -- h, ℓ, Z_R, a

          Press C. The value for $I_{\overset{\bullet}{E}}$ is displayed and stored in location 29.

D. Knock-on current, I_{knock} (amp)

     Cable inputs needed -- ℓ, a

          Press D. The value for I_{knock} is displayed and stored in location 30.

72

E.   Direct drive current, I_{DD} (amp)

     Cable inputs needed -- ℓ

          Enter the value for the dipole moment P (C-cm/cal), obtained from EXCITE.

          Press <u>RST</u>.

          Press <u>R/S</u>. The value for I_{DD} is displayed and stored in location 31.

B.8   SAMPLE PROBLEM

X rays characterized by an 8-keV blackbody spectrum are incident on a 3-mil-thick aluminum box. The total incident fluence, ϕ_T^{in}, is 5 cal/m^2 and the pulse is characterized by a 12-nsec rise time and a FWHM of 20 nsec. Calculate the peak time rates of change of the electric field and space-charge dipole moment. Calculate the cable currents $I_{\dot{H}}$ and $I_{\dot{E}}$ for the configurations given in Figure B-1.
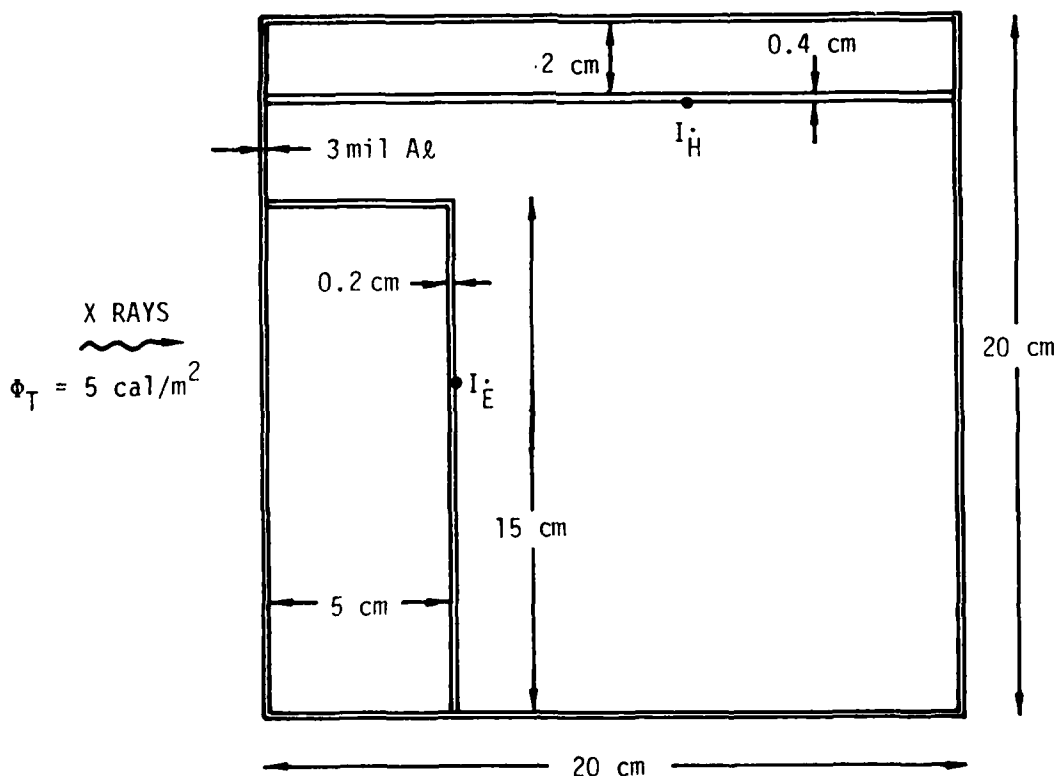
RE-03279

Figure B-1.   Sample problem configuration

This problem can be solved quickly and easily on the TI-59 calculator using the programs described in the previous sections. The method of solution involves the following five steps.

1. Generate an 8-keV blackbody spectrum using the program BLKBDY.

2. Attenuate the spectrum through 3 mils of aluminum using the program ATEN.

3. Calculate excitation parameters (electron emission yield and normal velocity) using the program EXCITE.

4. Calculate the response parameters (peak time rates of change of the electric field and space-charge dipole moment) using the program RESPONSE.

5. Couple these response parameters into the system and calculate cable currents using the program CABLE.

Step-by-step instructions used in solving this sample problem are given below for each of the five programs mentioned above. The five programs are to be executed sequentially since required input for one program is calculated and stored by the previous program. In general, if a mistake is made during input of parameters, it is safe to start over at the beginning of the calculational step after magnetic cards are read in for that step.

B.8.1   BLKBDY (see Section B.3)

Generate an 8-keV blackbody spectrum with total fluence $\phi_T^{in} = 5$ cal/m^2. An energy spectrum is specified by a curve of differential fluence, Φ (cal/cm^2-keV) versus energy, E (keV), and thus consists of (E_i, Φ_i) pairs. In general, the greater the number of pairs (bins), the more accurately a given spectrum can be represented. A maximum of 14 (E_i, Φ_i) pairs can be used in these programs, and if carefully chosen, is enough to accurately represent most spectra of interest. However, for this sample problem, only five (E_i, Φ_i) pairs, will be calculated, to shorten the time required to run through this example.

Enter	Press	Insert	Display	Comments
	CLR		0	
9	Op 17		239.89	Partition calculator
	CLR		0	
		BLKBDY	1.	Read in magnetic card*
5	A		5.	5 (E_i, Φ_i) pairs specified
8	B		1.	8-keV spectrum specified
5	C		5.	Total fluence $\Phi_T = 5$ cal/m^2
	E		.0130935239	Execute; calculates and stores (E_i, Φ_i) pairs

*The calculator occasionally has difficulty reading cards, especially if they were written by a different calculator. A flashing display at the end of this operation means that a read problem occurred, and the card should be inserted again after pressing CLR.

The generated spectrum which is stored in locations 60-88 can be examined as follows.

Enter	Press	Insert	Display	Comments
	RCL 60		3.2	E_1 (keV)
	RCL 61		24.	E_2 (keV)
	RCL 62		48.	E_3 (keV)
	RCL 63		72.	E_4 (keV)
	RCL 64		96.	E_5 (keV)
	RCL 65		0.	0. stored in location following final energy
	RCL 75		.0130935239	Φ_1 (cal/m^2-keV)
	RCL 76		.1423463343	Φ_2 (cal/m^2-keV)
	RCL 77		.0540071936	Φ_3 (cal/m^2-keV)
	RCL 78		.0090535248	Φ_4 (cal/m^2-keV)
	RCL 79		.0010683155	Φ_5 (cal/m^2-keV)

B.8.2 ATEN (see Section B.4)

Attenuate the 8-keV blackbody spectrum through 3 mils of aluminum. The density of aluminum is $\rho = 2.7$ g/cm^3, so τ, the mass per unit area, is calculated to be

$$\tau = (3 \times 10^{-3} \text{ inch})(2.54 \text{ cm/inch})(2.7 \text{ g/cm}^3),$$

$$\tau = 0.021 \text{ g/cm}^2.$$

Enter	Press	Insert	Display	Comments
	CLR		0	
		ATEN	1.	Read in magnetic card
	CLR		0	
		LOW Z	4.	Read in mag. card; Aℓ (Z=13), low-Z material
.021	A		.021	$\tau = 0.021$ g/cm^2
13	C		13	Atomic number for Aℓ, $Z = 13$
	E´		5.	Total incident fluence, $\Phi_T^{in} = 5$ cal/m^2
	E		0	Execute; the attenuated spectrum is calculated and stored
	E´		4.621826108	Total attenuated fluence, $\Phi_T^{attn} = 4.621826108$ cal/m^2

The attenuated spectrum is stored in locations 60-88 and can be examined as follows.

Enter	Press	Insert	Display	Comments
	RCL 60		3.2	E_1 (keV)
	RCL 61		24.	E_2 (keV)
	RCL 62		48.	E_3 (keV)
	RCL 63		72.	E_4 (keV)
	RCL 64		96.	E_5 (keV)
	RCL 65		0.	0. stored in location following final energy
	RCL 75		0.000000018	Φ_1^{attn} (cal/m^2-keV)
	RCL 76		.1378648063	Φ_2^{attn} (cal/m^2-keV)
	RCL 77		.0537916668	Φ_3^{attn} (cal/m^2-keV)
	RCL 78		.0090428046	Φ_4^{attn} (cal/m^2-keV)
	RCL 79		.0010677817	Φ_5^{attn} (cal/m^2-keV)

B.8.3   EXCITE (see Section B.5)

Calculate the forward electron emission yield and average normal velocity in the following manner.

Enter	Press	Insert	Display	Comments
	CLR		0	
		EXCITE	1.	Read in magnetic card
	CLR		0	
		YIELD (for velocity calculation)	3.	Read in magnetic card; yield data base (for velocity calculation)
	RST		3.	
	R/S		4.621826108	Total fluence of spectrum in locations 60-88
	R/S		.0000000745	Yield per unit total fluence
	R/S			Store yield (ignore display)
	CLR		0	
		$\dfrac{\text{YIELD}}{\text{VELOCITY}}$	3.	Read in mag. card, yield/velocity, data base
	RST		3.	
	R/S		4.621826108	Total fluence of spectrum in locations 60-88
	R/S		1.5368727-15	Yield/velocity per unit total fluence
	R/S		48447820.7	Yield/(yield/velocity) = velocity
	CLR		0	
		FORWARD YIELD ALUMINUM	3.	Read in magnetic card, forward yield data base for aluminum
	RST		3.	
	R/S		4.621826108	Total fluence of spectrum in locations 60-88
	R/S		.0000000745	Yield per unit total fluence

Results:

Average normal velocity = 48447820.7 m/sec = 4.84×10^7 m/sec

$$\text{Yield per unit incident fluence} = \frac{\text{yield}}{\text{attenuated fluence}} \; \frac{\text{attenuated fluence}}{\text{incident fluence}}$$

$$= \frac{\text{yield}}{\text{incident fluence}} = (.0000000745) \frac{4.621826108}{5.0}$$

$$= 6.89 \times 10^{-8} \text{ C/cal}$$

77

B.8.4 RESPONSE (see Section B.6)

Calculate the peak time rate of change of the electric field $\dot{E}$ and the peak time rate of change of the space-charge dipole moment $\dot{P}$.

Enter	Press	Insert	Display	Comments
	CLR		0	
5	Op 17		559.49	
	CLR		0	
		RESPONSE (Bank 1)	1.	Read in magnetic card.
	CLR		0	
		RESPONSE (Bank 2)	2.	Read in magnetic card.
	CLR		0	
		RESPONSE (Bank 3)	3.	Read in magnetic card.
12 EE			12 00	
9	+/-		12-09	
	STO 10		1.2-08	Pulse rise time, t_R (sec).
20	EE		20 00	
9	+/-		20-09	
	STO 12		2.0-08	FWHM, Δt (sec).
5	STO 13		5.00	Φ Total incident fluence (cal/m^2)
6.89	EE		6.89 00	
8	+/-		6.89-08	
	STO 16		6.89-08	Yield per incident fluence, Y (C/cal-m^2).
4.84	EE		4.84 00	
7	STO 17		4.84 07	Average normal velocity, v (m/sec).
	RST		4.84 07	
	R/S		8.3369 08	Execute.

The calculated response parameters can be examined as follows.

Enter	Press	Insert	Display	Comments
	CLR		0	
	RCL 15		17.225	Peak emission current, J_{em} (amp/m^2).
	RCL 20		9.307368187	Peak time rate of change of space-charge dipole moment (amp/m).
	RCL 21		833690000.	Peak time rate of change of $\dot{P}$, $\ddot{P}$ (amp/m-sec).
	RCL 22		1.9454484 12	Peak time rate of change of electric field, $\dot{E}$ (V/m-sec).
	RCL 23		0.	For $t_{m3} > \Delta t$, program sets E = 0.
	RCL 18		0.	Since value is zero, use t_{m2} as time of peak $\dot{P}$.
	RCL 19		.0000000228	Time of peak $\dot{P}$, t_{m2} = 22.8 nsec.
	RCL 26		.0000000324	Time of peak $\dot{E}$ = 32.4 nsec.

B.8.5   CABLE (see Section B.7)

Calculate the cable currents $I_{\dot{H}}$ and $I_{\dot{E}}$ for the configuration in Figure B-1.

Enter	Press	Insert	Display	Comments
	CLR		0	
		CABLE (Bank 1)	1.	Read in magnetic card.
	CLR		0	
		CABLE (Bank 2)	2.	Read in magnetic card.
.02	A´		0.02	Cable standoff, h (m).
.2	C´		2. -01	Cable length, ℓ (m).
0	D´		0. 00	Termination impedance, Z_R (ohm).
.002	E´		2. -03	Cable radius, a (m).
.2	E		2. -01	Cavity diameter, 2R (m).
	B´		3.6157638-02	$I_{\dot{H}}$ (amp).
.05	A´		5. -02	Cable standoff, h (m).
.15	C´		1.5 -01	Cable length, ℓ (m).
.001	E´		1. -03	Cable radius, a (m).
	C		1.762642-01	$I_{\dot{E}}$ (amp)

Results:

$$I_{\dot{H}} = 0.04 \text{ amp}$$

$$I_{\dot{E}} = 0.18 \text{ amp}$$

B.8.6   Bin Selection

As mentioned earlier, a large number of bins [i.e., (E_i, Φ_i) pairs] may be required to accurately represent a given spectrum. In this sample problem, only five bins were specified to save time. For comparison, the same sample problem was run specifying 14 bins in BLKBDY. Results of these two calculations are given below.

Result	5 bins	14 bins
Average velocity (m/sec)	4.84×10^7	3.72×10^7
Yield (C/cal)	6.89×10^{-8}	1.12×10^{-7}
J_{em}	17.225	28.
$\dot{P}$	9.31	7.92
$\ddot{P}$	8.34×10^8	7.62×10^8
$\dot{E}$	1.95×10^{12}	3.16×10^{12}
$I_{\dot{H}}$	0.04	0.06
$I_{\dot{E}}$	0.18	0.29

There are definite differences between the results of these two calculations, and it is emphasized that the user must select bins with care.

APPENDIX C

PHOTOEMISSION EXCITATION PARAMETER DATA BASE

This appendix contains graphs of the photoemisson excitation parameter data base employed in the calculator programs. The materials and excitation parameters for which data are provided on magnetic cards are listed in Table C-1. The average normal electron velocity is only a weak function of the emission material and direction, and in fact, the forward-directed emission data for aluminum is representative, within a factor of 2, of every material for both forward and backward directions. The dipole moment data are provided for representative cable shield materials. Extension of the data base to other materials and parameters can be performed straightforwardly as the need arises. Relevant quantities such as dose and electron range can be included, for example.

Results for electron yield, average normal velocity, and dipole moment in dielectric materials are plotted in Figures C-1 through C-7 as a function of in-and-out x-ray energy over the range 1 to 1000 keV. The curves were obtained from the QUICKE2 electron emission code for monoenergetic x-ray spectra, and are fit to within a factor of 2 over the energy range using power-law interpolation in the calculator. As many as 14 point pairs in both the x-ray spectrum and the data base are interpolated and convolved by the EXCITE program (see Appendix B) to obtain the total quantity for a given spectrum. The units of electron yield and dipole moment are presented as coulombs per calorie and coulomb-meters per calorie. The yield is actually coulombs per unit area per calorie per unit area, which reduced to coulombs per calorie. The dipole moment can be thought of similarly.

Table C-1. Materials and Excitation Parameters Available
on Magnetic Cards for the TI-59 Calculator Program EXCITE

| Material | Photo-Electron Yield | | Average Normal Velocity | Dipole Moment in Low-Z Material | |
	Forward	Reverse		Forward	Reverse
Carbon	x	x			
Aluminum	x	x		x	x
Copper	x	x		x	x
Silver	x	x		x	x
Gold	x	x			
Mylar	x	x			
Fiberglass	x	x			
Quartz	x	x			

Data for aluminum forward emission fits forward and reverse emission for all materials within a factor of 2.
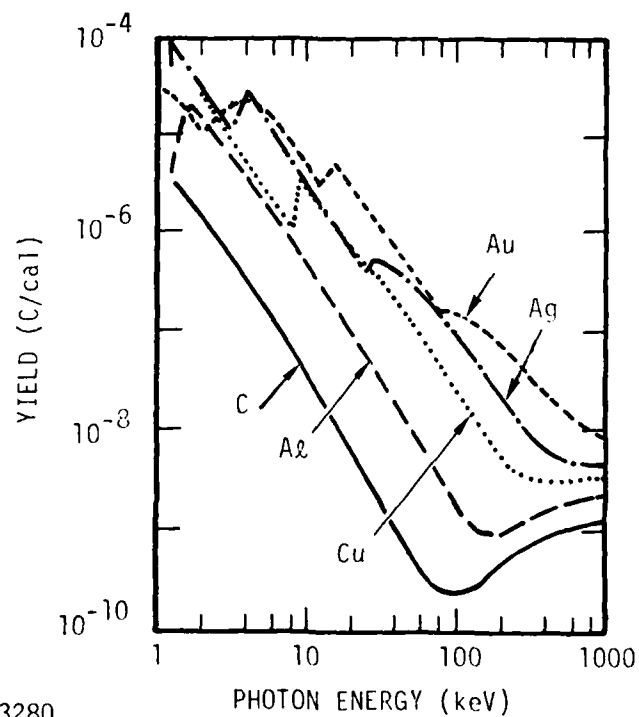
RE-03280

Figure C-1. Reverse-emitted photoelectron yield versus
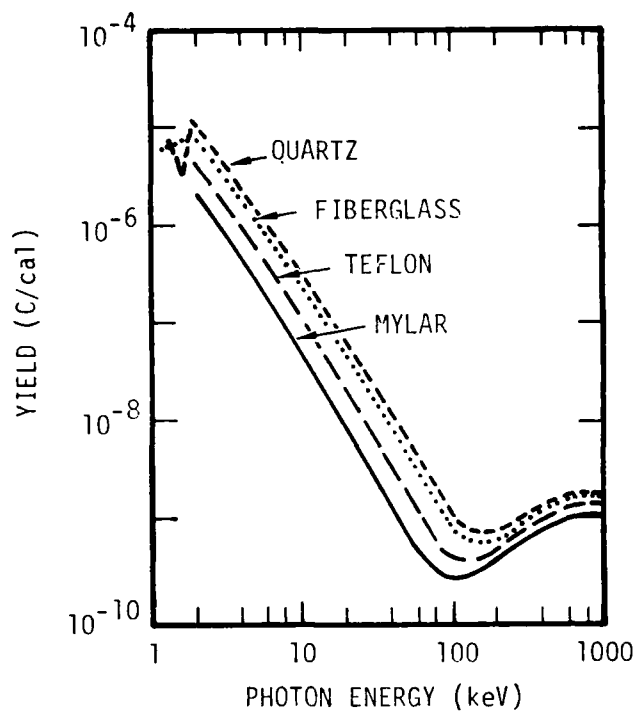monoenergetic x-ray energy for representative elements

82

Figure C-2. Reverse-emitted photo-electron yield versus monoenergetic x-ray energy for representative satellite materials
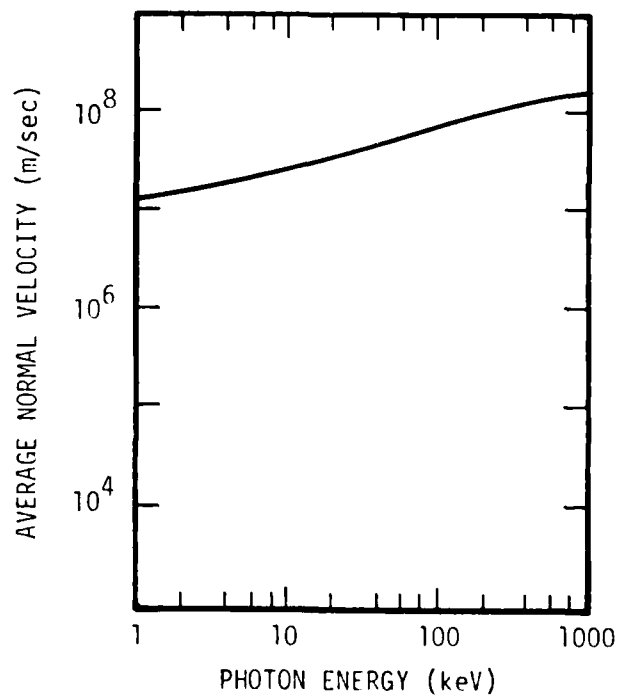
RE-03281

Figure C-3. Electron average normal velocity versus monoenergetic x-ray energy used to represent all elements and satellite materials for forward and reverse electron emission

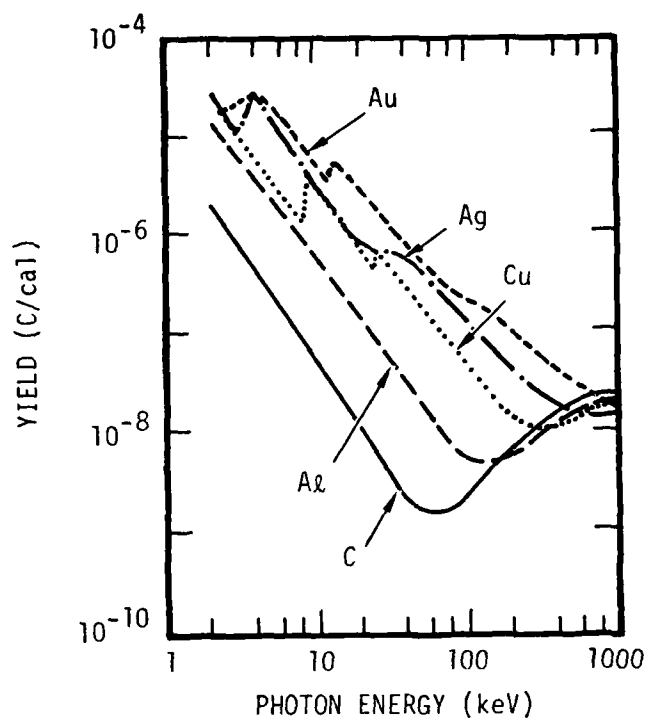RE-03282

Figure C-4. Forward-emitted photo-electron yield versus monoenergetic x-ray energy for elements

RE-03283

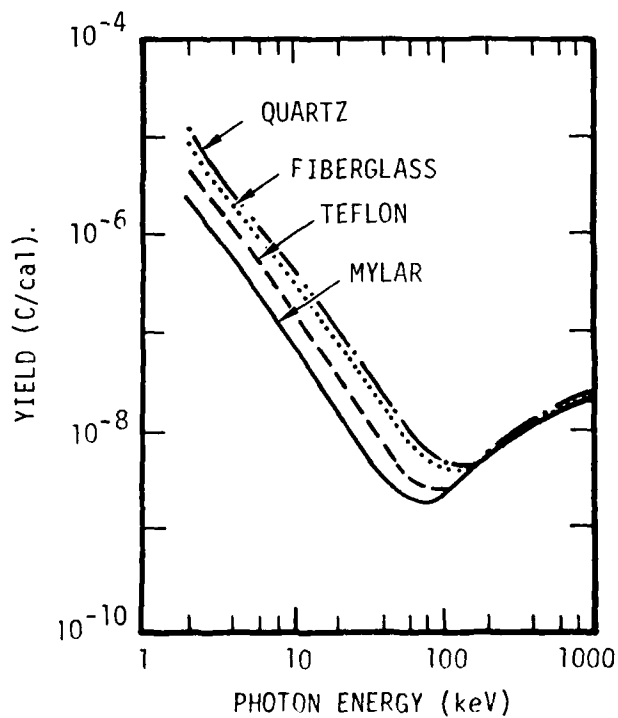Figure C-5. Forward-emitted photo-electron yield versus monoenergetic x-ray energy for representative satellite materials
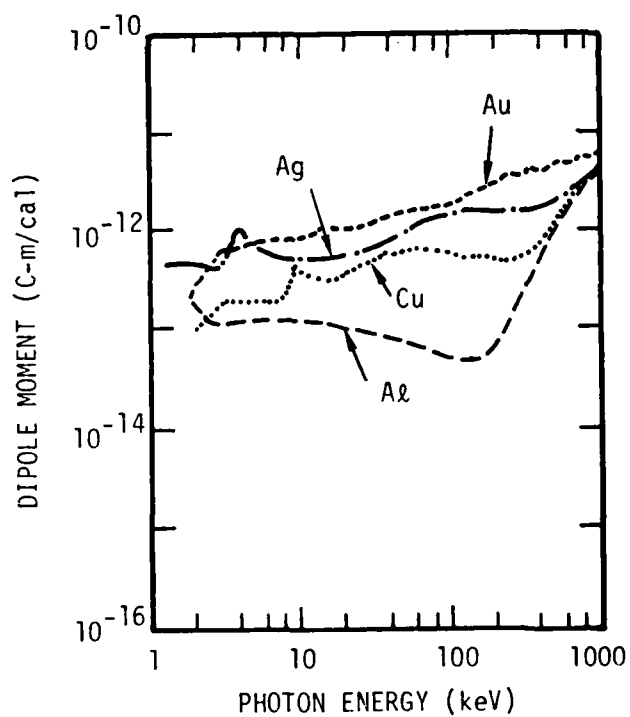
RE-03284

Figure C-6. Forward-emitted photo-electron dipole moment versus monoenergetic x-ray energy for representative elements
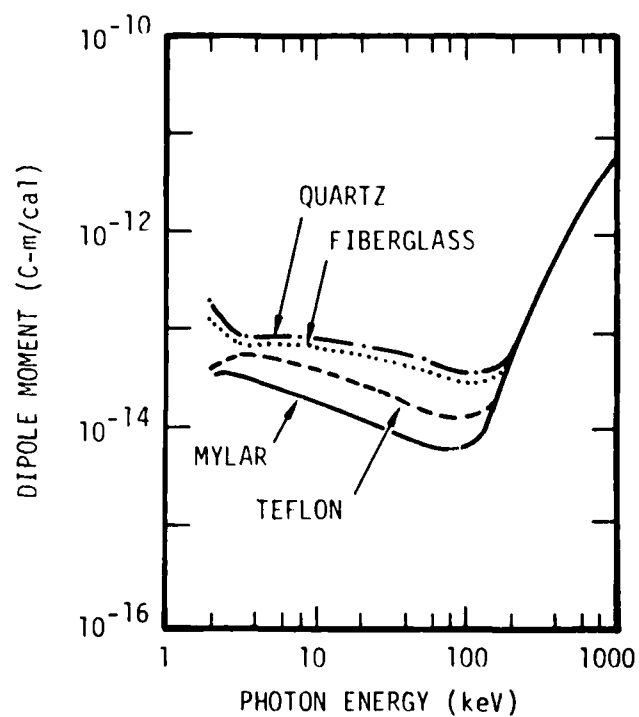
RE-03285

Figure C-7. Forward-emitted photo-electron dipole moment versus monoenergetic x-ray energy for representative satellite materials

RE-03286

DEPARTMENT OF DEFENSE

Assistant to the Secretary of Defense
Atomic Energy
    ATTN: Executive Assistant

Defense Communications Agency
    ATTN: DWSE-E, B. Hoff

Defense Communications Engineer Center
    ATTN: Code R401, T. Ellington

Defense Intelligence Agency
    ATTN: DB-4C

Defense Nuclear Agency
2 cy ATTN: RAEV
4 cy ATTN: TITL

Defense Technical Information Center
12 cy ATTN: DD

Field Command
Defense Nuclear Agency
    ATTN: FCP, J. T. McDaniel
    ATTN: FCLMC, H. R. Putnam
    ATTN: FCTO
    ATTN: FCTT
    ATTN: FCTT, W. Summa
    ATTN: FCTP
    ATTN: FCTXE

Field Command
Defense Nuclear Agency
Livermore Branch
    ATTN: FCPRL

Field Command
Defense Nuclear Agency
Los Alamos Branch
    ATTN: FCPRA

Field Command Test Directorate
Test Construction Division
Defense Nuclear Agency
    ATTN: FCTC

Interservice Nuclear Weapons School
    ATTN: TTV

Joint Chiefs of Staff
    ATTN: J-5, Nuclear Division
    ATTN: C3S, Evaluation Office

Joint Strat Tgt Planning Staff
    ATTN: JLTW-2
    ATTN: JLA

National Communications System
    ATTN: NCS-TS

Under Secretary of Defense for Rsch & Engrg
    ATTN: Strategic & Space Sys (OS)
    ATTN: AE

DEPARTMENT OF THE ARMY

BMD Advanced Technology Center
Department of the Army
    ATTN: ATC-O

BMD Systems Command
Department of the Army
    ATTN: BDMSC-H

Deputy Chief of Staff for Rsch Dev & Acq
Department of the Army
    ATTN: DAMA-CSS-N

Electronics Tech & Devices Lab
U.S. Army Electronics R&D Command
    ATTN: DRSEL

Harry Diamond Laboratories
Department of the Army
    ATTN: DELHD-N-RBC, R. Gilbert
    ATTN: DELHD-I-TL

U.S. Army Communications Sys Agency
    ATTN: CCM-AD-LB

U.S. Army Foreign Science & Tech Ctr
    ATTN: DRXST-IS-1

U.S. Army Missile Command
    ATTN: RSIC

DEPARTMENT OF THE NAVY

Naval Research Laboratory
    ATTN: Code 7550, J. Davis
    ATTN: Code 6701
    ATTN: Code 6707, K. Whitney

Naval Surface Weapons Center
    ATTN: Code F31

Strategic Systems Project Office
Department of the Navy
    ATTN: NSP

DEPARTMENT OF THE AIR FORCE

Air Force Geophysics Laboratory
    ATTN: PH, C. Pike

Air Force Weapons Laboratory
Air Force Systems Command
    ATTN: SUL
    ATTN: NT
    ATTN: NTSW, Col Bloemker
2 cy ATTN: NTYC

Air University Library
Department of the Air Force
    ATTN: AUL/LSE

DEPARTMENT OF THE AIR FORCE (Continued)

Ballistic Missile Office
Air Force Systems Command
        ATTN: ENMG
        ATTN: SYDT
        ATTN: ENSN

Deputy Chief of Staff
Research, Development, & Acq
Department of the Air Force
        ATTN: AFRDQI

Headquarters Space Division
Air Force Systems Command
        ATTN: YKD

Headquarters Space Division
Air Force Systems Command
        ATTN: YNV

Rome Air Development Center
Air Force Systems Command
        ATTN: ESR, E. Burke

Strategic Air Command
Department of the Air Force
        ATTN: XPFS
        ATTN: NRI-STINFO, Library

OTHER GOVERNMENT AGENCIES

Central Intelligence Agency
        ATTN: OSWR/STD/MTB, A. Padgett

Department of Commerce
National Oceanic & Atmospheric Admin
        ATTN: F. Fehsenfeld

NASA
Lewis Research Center
        ATTN: Library
        ATTN: N. Stevens
        ATTN: C. Purvis

DEPARTMENT OF ENERGY CONTRACTORS

Lawrence Livermore National Lab
        ATTN: Technical Info Dept, Library

Los Alamos National Laboratory
        ATTN: MS 364

Sandia National Laboratories
Livermore Laboratory
        ATTN: T. Dellin

Sandia National Lab
        ATTN: 3141

DEPARTMENT OF DEFENSE CONTRACTORS

Aerospace Corp
        ATTN: V. Josephson
        ATTN: Library

Avco Research & Systems Group
        ATTN: Library A830

DEPARTMENT OF DEFENSE CONTRACTORS (Continued)

Beers Associates, Inc
        ATTN: B. Beers

Computer Sciences Corp
        ATTN: A. Schiff

Dikewood Corporation
        ATTN: Technical Library

Dikewood Corporation
        ATTN: K. Lee

EG&G Wash Analytical Svcs Ctr, Inc
        ATTN: Library

Ford Aerospace & Communications Corp
        ATTN: A. Lewis

General Electric Co
        ATTN: J. Peden

Hughes Aircraft Co
        ATTN: Technical Library

Hughes Aircraft Co
        ATTN: E. Smith
        ATTN: W. Scott
        ATTN: A. Narevsky

Institute for Defense Analyses
        ATTN: Classified Library

IRT Corp
        ATTN: N. Rudie
        ATTN: B. Williams
        ATTN: Library

JAYCOR
        ATTN: Library
4 cy ATTN: E. Wenaas
4 cy ATTN: A. Woods
4 cy ATTN: R. Leadon
4 cy ATTN: B. Nichols
4 cy ATTN: K. Brannon

JAYCOR
        ATTN: R. Sullivan

JAYCOR
        ATTN: R. Poll

Johns Hopkins University
        ATTN: P. Partridge

Kaman Sciences Corp
        ATTN: Library
        ATTN: W. Rich
        ATTN: N. Beauchamp
        ATTN: D. Osborn

Kaman Tempo
        ATTN: W. McNamara
        ATTN: DASIAC

Lockheed Missiles & Space Co, Inc
        ATTN: Dept 85-85

88

DEPARTMENT OF DEFENSE CONTRACTORS (Continued)

McDonnell Douglas Corp
    ATTN: R. Kloster

McDonnell Douglas Corp
    ATTN: S. Schneider

Mission Research Corp
    ATTN: C. Longmire
    ATTN: M. Scheibe
    ATTN: R. Stettner

Mission Research Corp
    ATTN: B. Goplen

Mission Research Corp, San Diego
    ATTN: Library
    ATTN: V. Van Lint

Mission Research Corporation
    ATTN: W. Ware

Pacific-Sierra Research Corp
    ATTN: L. Schlessinger
    ATTN: H. Brode

R & D Associates
    ATTN: S. Siegel
    ATTN: Technical Information Center
    ATTN: P. Haas

DEPARTMENT OF DEFENSE CONTRACTORS (Continued)

Rockwell International Corp
    ATTN: Library

Science Applications, Inc
    ATTN: W. Chadsey

Science Applications, Inc
    ATTN: D. Woodward
    ATTN: K. Sites

Spire Corp
    ATTN: R. Little

SRI International
    ATTN: Library

Systems, Science & Software, Inc
    ATTN: A. Wilson
    ATTN: Library

Teledyne Brown Engineering
    ATTN: I. Ford

TRW Defense & Space Sys Group
    ATTN: D. Clement
    ATTN: Technical Information Center